
GOODNESS-OF-FIT TESTS FOR SPATIAL POINT PROCESSES: A POWER STUDY

A PREPRINT

Chiara Fend

Department of Mathematics
RPTU University Kaiserslautern-Landau
Kaiserslautern, Germany
chiara.fend@rptu.de

Claudia Redenbach

Department of Mathematics
RPTU University Kaiserslautern-Landau
Kaiserslautern, Germany
claudia.redenbach@rptu.de

May 19, 2025

ABSTRACT

Spatial point processes are used as models in many different fields ranging from ecology and forestry to cosmology and materials science. In recent years, model validation, and in particular goodness-of-fit testing of a proposed point process model have seen many advances. Most of the proposed tests are based on a functional summary statistic of the observed pattern. In this paper, the empirical powers of many possible goodness-of-fit tests that can be constructed from such a summary statistic are compared in an extensive simulation study. Recently introduced functional summary statistics derived from topological data analysis and new constructions for the test statistic such as the continuous ranked probability score are included in the comparison. We discuss the performance of specific combinations of functional summary statistic and test statistic and their robustness with respect to other tuning parameters. Finally, tests using more than one individual functional summary statistic are also investigated. The results allow us to provide guidelines on how to choose powerful tests in a particular test setting.

Keywords goodness-of-fit · spatial point process · monte carlo test · second-order statistics · topological data analysis · global envelope test

1 Introduction

In Fend and Redenbach (2025), a general framework for the goodness-of-fit testing of spatial point processes was introduced. The reviewed goodness-of-fit tests are based on functional summary statistics of the point pattern. Several choices for these statistics are available, going from classical approaches such as Ripley's K -function to recent descriptors derived from topological data analysis. Each test in the framework is composed of a functional summary statistic, a test statistic, and an ordering that measures how extreme an observation is. Here, we present an extensive empirical investigation of the power of goodness-of-fit tests that fit the framework of Fend and Redenbach (2025). In particular, we include combinations of the individual components that have, to the best of our knowledge, not yet been considered. We compare only Monte Carlo tests, i.e. we use simulations of the null model and their empirical functional summaries to decide if the observed value of the test statistic is extreme or not. Asymptotic theory for point processes has seen many developments in the last years, but it is still limited to restricted classes of point processes and particular summary functions and test statistics. This is the reason why we excluded asymptotic tests from this investigation.

Several previous power studies on goodness-of-fit testing for spatial point processes were reviewed in Section 7 of Fend and Redenbach (2025). Although most studies concentrate on the null hypothesis of complete spatial randomness (CSR), the general setting differs widely, as very different models and parameter choices were used to simulate the observed data. Consequently, combining and comparing results from these studies is not straightforward. In addition, many possible tests that can be built from the general framework have to be tested. Examples are the use of the continuous ranked probability score as test statistic or topological data analysis based summary statistics in the Monte Carlo setting.

The main focus of our study is on the combination of summary statistic, test statistic, and ordering. We test the null hypothesis of complete spatial randomness, as this is the most common hypothesis in the literature. In order to investigate the empirical power of the test for different types of deviations from CSR, we consider five point process models, namely a Matérn cluster point process, the Baddeley-Silverman cell process, a Hardcore process, a Gaussian determinantal point process and a Strauss process.

The reminder of this work is organized as follows. In Section 2 we provide a small introduction to the individual components of the goodness-of-fit tests. Recommendations obtained from prior studies and remaining open questions are summarized in Section 3. The set up of our simulation study is described in Section 4. Section 5 presents the results of the simulation study. The paper concludes with a discussion of the open questions in Section 6.

2 General framework for goodness-of-fit tests

In this section we briefly present the framework for goodness-of-fit tests that was introduced in Fend and Redenbach (2025). For a detailed introduction we refer the reader to this review article.

Let \mathbf{X} be a spatial point process on \mathbb{R}^d , $d > 1$. We assume that \mathbf{X} is simple, which means that the points are almost surely pairwise distinct. The point process is then given as the random set $\mathbf{X} = \{X_1, \dots, X_N\}$ where $N \in \mathbb{N} \cup \{\infty\}$. Additionally, we assume stationarity and isotropy of the point process, which means that the distribution of the process is invariant under translations and rotations around the origin. The intensity $\lambda > 0$ of a stationary point process \mathbf{X} is the expected number of points per unit volume. We have $\mathbb{E}[\mathbf{X}(B)] = \mathbb{E}[\#\{X_1, \dots, X_N\} \cap B] = \lambda |B|$ for every Borel set $B \in \mathcal{B}^d$, where $|\cdot|$ denotes the Lebesgue measure on $(\mathbb{R}^d, \mathcal{B}^d)$ and $\#A$ the cardinality of the countable set A .

A realization of \mathbf{X} is a so-called point pattern \mathbf{x} . We observe \mathbf{x} only within a bounded observation window $W \subset \mathbb{R}^d$ with $0 < |W| < \infty$. The observed pattern is denoted as $\mathbf{x}_0 = \mathbf{x} \cap W = \{x_1, \dots, x_n\}$ for $n \in \mathbb{N}$.

In the following, let $B_r(x) = \{y \in \mathbb{R}^d \mid \|y - x\| \leq r\}$ be the Euclidean ball with radius r centered in $x \in \mathbb{R}^d$. The indicator function of a set A is denoted as $\mathbb{1}(\cdot \in A)$.

Based on the observation \mathbf{x}_0 of the point process \mathbf{X} with unknown distribution P we test the hypothesis

$$H_0 : P = P_0 \quad \text{vs.} \quad H_1 : P \neq P_0.$$

For simplicity, we assume that P_0 is a fully specified point process model, which means that no parameters have to be estimated from the observed pattern. We refer the reader to Fend and Redenbach (2025) for the case of composite hypotheses.

In general, a test will be constructed using the following components:

1. A functional summary statistic $T(\mathbf{X}, \cdot) : \mathcal{R} \rightarrow \mathbb{R}$ where $\mathcal{R} \subset \mathbb{R}$ and its nonparametric estimator $\hat{T}(\mathbf{x}_0, \cdot) : \mathcal{R} \rightarrow \mathbb{R}$.
2. A test statistic D that aggregates $\hat{T}(\mathbf{x}_0, \cdot)$ on the relevant subset \mathcal{R}^* of the domain \mathcal{R} . The test statistic D can be scalar or vector-valued and can potentially be based on pointwise deviations from the null model.
3. An ordering \preceq on the range of D that defines what is considered extreme under the null hypothesis. In our notation $D_k \preceq D_l$ means that D_k is at least as extreme as D_l , thus small values indicate extremeness.
4. A method for computing the critical value, either via asymptotic reasoning or by Monte Carlo simulation.

Not every test statistic is suitable for every ordering such that we introduce the possible choices always in pairs. As mentioned in the introduction, we restrict our study to Monte Carlo tests.

For this testing procedure, we sample m point patterns $\mathbf{x}_1, \dots, \mathbf{x}_m$ from P_0 . Let D_0, \dots, D_m denote the values of the selected test statistic for $\mathbf{x}_0, \dots, \mathbf{x}_m$. We reject H_0 if the Monte Carlo p -value defined as

$$p_{\text{MC}} = \frac{1}{m+1} \left(1 + \sum_{i=1}^m \mathbb{1}(D_i \preceq D_0) \right)$$

is smaller than or equal to the selected significance level $\alpha \in (0, 1)$.

From the literature, it is well known that a single summary statistic cannot fully describe the distribution of a point process. The two-step procedure of global envelope tests within the R-package GET (Myllymäki and Mrkvička, 2024) allows to combine $1 < K < \infty$ different individual functional summary statistics into one overall goodness-of-fit test.

In the first step, we proceed with components 1 - 3 from above for each individual summary statistic T_1, \dots, T_K . For every summary statistic T_k , we summarize the result of the ordering in a scalar number d_k . This can be done, e.g., in terms of the scalar-valued test statistic or via the value of the depth measure that induces the ordering of a vector-valued test statistic. Note that we require that for all individual values d_1, \dots, d_K only small values are considered extreme.

In the second step, we define the vector $D = [d_1, \dots, d_K]^T \in \mathbb{R}^K$ as final test statistic. Then we continue with components 3 and 4 of the Monte Carlo test with the vector-valued test statistic. The ordering \preceq in the two-step procedure is always induced by the extreme rank length measure (Myllymäki et al., 2017) with one-sided pointwise extremeness. More details on the two-step procedure and alternative approaches to combining functional summary statistics in a goodness-of-fit test setting can be found in Fend and Redenbach (2025, Section 6.4).

2.1 Functional summary statistic

There exist several functional summary statistics that can be used for goodness-of-fit tests and that consider different properties of the point process. A detailed theoretical introduction into the classical (probabilistic) functional summary statistics can be found in Baddeley et al. (2015) and Møller and Waagepetersen (2003). The topological functional summary statistics are introduced in Fend and Redenbach (2025).

The list of the functional summary statistics that are of interest in our simulation study in Section 4 as well as the nonparametric estimators that we used can be found in Table 1. To understand the construction of the estimators, further notation is necessary, which we introduce below.

The domain \mathcal{R} of all eleven functional summary statistics is given as a subset of $\mathbb{R}_{\geq 0}$. The evaluation point $r \in \mathcal{R}$ then denotes a spatial range or distance within the point pattern.

In case of Ripley's K -function and the L -function we use Ripley's isotropic edge correction estimator. The edge correction factor $p_W(x_1, \|x_1 - x_2\|)$ is the probability that given the first point x_1 , the second point x_2 lying on $\partial B(x_1, \|x_1 - x_2\|)$ falls into the observation window W . The exact formula of $p_W(x_1, \|x_1 - x_2\|)$ can be found in Baddeley et al. (2015, Sec. 7.4.4). For the transformation of the K -function into the L -function we additionally need the volume ω_d of the d -dimensional unit ball, e.g., if $d = 2$ we have $\omega_2 = |B_1(0)| = \pi$.

Since the pair-correlation function is a density, it is estimated using a kernel estimator. The function k_b hereby denotes the Epanechnikov kernel with bandwidth b , see Baddeley et al. (2015, Sec. 7.6.2). Furthermore, the factor σ_d denotes the surface area of the ball with radius 1 in \mathbb{R}^d , e.g., $\sigma_2 = 2\pi$.

In case of the distance-based functional summary statistics F , G and J , we use the Kaplan-Meier style edge corrections discussed in Baddeley et al. (2015, Sec. 8.11.4). For the nearest neighbor distance distribution function G let $d_{nn}(x_i) = d(x_i, \mathbf{x}_0 \setminus \{x_i\})$ be the distance from x_i to its nearest neighbor in \mathbf{x}_0 . The so-called observed failure distance of x_i is defined as $t(x_i) = \min\{d_{nn}(x_i), d(x_i, \partial W)\}$. For estimation of the empty space function, the points x_i are replaced by test locations u in a regular lattice $\text{Lat} \subset W$. A test position $u \in \text{Lat}$ takes on the role of the observed point x_i in the G -function estimator. Thus, we have $d_{nn}(u) = d(u, \mathbf{x}_0)$ and $t(u) = \min\{d_{nn}(u), d(u, \partial W)\}$.

For the five topological functional summary statistics, we use the alpha-complex filtration of the observed point pattern \mathbf{x}_0 which is a filtration of the Delaunay triangulation. The alpha-complex at distance $r > 0$ is given as

$$\mathcal{K}_r = \{\sigma \text{ simplex with vertices in } \mathbf{x}_0 \mid \bigcap_{x_i \in V(\sigma)} (B_r(x_i) \cap \text{Voronoi}(x_i, \mathbf{x}_0)) \neq \emptyset\}$$

where $\text{Voronoi}(x_i, \mathbf{x}_0)$ denotes the Voronoi cell of the point x_i with respect to the entire point pattern \mathbf{x}_0 and $V(\sigma)$ the set of vertices of the simplex. The set of p -dimensional topological features of the filtration is denoted by J^p for $p \in \mathbb{N}_0$. The 0-dimensional features are the connected components, the 1-dimensional features are circular loops, and the 2-dimensional features are voids in space. Each topological feature j has a birth time b_j that corresponds to the time it first appeared in the filtration and a death time d_j corresponding to the last occurrence.

From the functional summary statistics introduced in Fend and Redenbach (2025), we do not include the variance-stabilizing arcsin-transformation of G called G^* as it is rarely used in practice. The topological summary function ND_0 is also excluded as it is by definition the complement of the 0-dimensional Betti curve, the latter being the better known standard topological characteristic.

2.2 Test statistic and ordering

For the test statistic, we generally distinguish three categories in the framework. Type A statistics are scalar-valued and based on summarizing the absolute pointwise deviations between the empirical functional summary statistic of

T	Name	Estimator $\hat{T}(\mathbf{x}_0, r)$	Equation
K	Ripley's K -function	$\frac{ W }{n(n-1)} \sum_{x_1, x_2 \in \mathbf{x}_0}^{\neq} \frac{\mathbb{1}(\ x_1 - x_2\ \leq r)}{p_W(x_1, \ x_1 - x_2\)}$	(1)
L	L -function	$\left(\hat{K}(\mathbf{x}_0, r)/\omega_d\right)^{\frac{1}{d}}$	(2)
pcf	pair correlation function	$\frac{ W }{\sigma_d r^{d-1} n(n-1)} \sum_{x_1, x_2 \in \mathbf{x}_0}^{\neq} \frac{k_b(r - \ x_1 - x_2\)}{p_W(x_1, \ x_1 - x_2\)}$	(4)
F	Empty space function	$1 - \prod_{s \leq r} \left(1 - \frac{\#\{u \in \text{Lat} \mid t(u) = s, d_{nn}(u) \leq t(u_i)\}}{\#\{u \in \text{Lat} \mid t(u) \geq s\}}\right)$	(5)
G	Nearest neighbor distance distribution function	$1 - \prod_{s \leq r} \left(1 - \frac{\#\{x_i \in \mathbf{x}_0 \mid t(x_i) = s, d_{nn}(x_i) \leq t(x_i)\}}{\#\{x_i \in \mathbf{x}_0 \mid t(x_i) \geq s\}}\right)$	(6)
J	J -function	$(1 - \hat{G}(\mathbf{x}_0, r))/(1 - \hat{F}(\mathbf{x}_0, r))$	(8)
β_0	0-dimensional Betti curve	$\sum_{j \in J^0} \mathbb{1}(b_j \leq r, d_j > r)$	(14)
β_1	1-dimensional Betti curve	$\sum_{j \in J^1} \mathbb{1}(b_j \leq r, d_j > r)$	(14)
APF_0	0-dimensional accumulated persistence function	$\sum_{j \in J^0} d_j \mathbb{1}(d_j \leq r)$	(15)
APF_1	1-dimensional accumulated persistence function	$\sum_{j \in J^1} (d_j - b_j) \mathbb{1}(b_j \leq r)$	(16)
χ	Euler characteristic curve	$\sum_{\sigma \in \mathcal{K}_r} (-1)^{\#V(\sigma)-1}$	(18)

Table 1: List of the functional summary statistics appearing in the simulation study. The equation numbers refer to the corresponding equation in Fend and Redenbach (2025) that introduces the theoretical counterpart.

the observed point pattern and the reference value under the null hypothesis. The reference value is either the true functional summary statistic of the null model at that point or an estimate obtained from a set of simulations of the null model. Since type A test statistics involve absolute pointwise deviations to the null, only large values of the test statistic are extreme. In this category, we find the maximum absolute deviation (Diggle, 1979), the integrated squared deviation (Diggle, 1979; Cressie, 1993; Loosmore and Ford, 2006), the scaling approaches of Myllymäki et al. (2015) and the integrated continuous ranked probability score (Heinrich-Mertsching et al., 2024).

All test statistics that are scalar-valued and do not use pointwise deviations belong to type B. Extremeness is two-sided in this case, as both larger and smaller values than under the null are significant. A point evaluation of the summary function was used by Ripley (1977) and Diggle (1979) for pointwise envelopes. The integral of an empirical functional summary statistic is used in many asymptotic tests.

The third type C involves test statistics that are not scalar-valued. In most cases, the test statistic is vector-valued and contains the empirical functional summary statistic at a finite number of evaluation points. Extremeness of the vectors in a Monte Carlo test is measured using a statistical depth function that induces an ordering on the set of vectors that are obtained through the simulations. This category allows us to include the global envelope tests of Myllymäki et al. (2017) in our framework. The second test statistic in this group is the pointwise continuous ranked probability score based on Heinrich-Mertsching et al. (2024).

Table 2 provides a list of test statistics and the possible orderings that we used in our simulation study. The relevant part of the domain $\mathcal{R}^* \subset \mathcal{R} \subseteq \mathbb{R}_{\geq 0}$ over which one integrates or takes the supremum is in most cases an interval $[r_{\min}, r_{\max}]$. The *optimal* choices for the bounds depend on the selected functional summary statistic, the type of observed point pattern, and the observation window. For several summary function estimators listed in Table 1 there are

computational restrictions due to denominators that could potentially be zero if the upper bound r_{\max} is chosen too large. The estimator for the pair correlation function generally has a poor performance for r close to 0 (Baddeley et al., 2015). In that case, setting $r_{\min} > 0$ is necessary. For all other functional summary statistics, we can set $r_{\min} = 0$. The only test statistic that does not require an interval \mathcal{R}^* is the POINT test statistic, as it uses only a single evaluation point r^* .

Type	Statistic	Formula	Ordering	Equations
A	MAD	$\sup_{r \in \mathcal{R}^*} \hat{T}(\mathbf{x}_0, r) - T(\mathbf{Y}, r) $	larger	(19), (32)
	DCLF	$\int_{\mathcal{R}^*} (\hat{T}(\mathbf{x}_0, r) - T(\mathbf{Y}, r))^2 dr$	larger	(20), (32)
	ST	$\sup_{r \in \mathcal{R}^*} \left \frac{\hat{T}(\mathbf{x}_0, r) - T(\mathbf{Y}, r)}{\text{sd}(\hat{T}(\mathbf{Y}, r))} \right $	larger	(21), (32)
	QDIR	$\sup_{r \in \mathcal{R}^*} \left\{ \mathbb{1}(\hat{T}(\mathbf{x}_0, r) \geq T(\mathbf{Y}, r)) \cdot \frac{\hat{T}(\mathbf{x}_0, r) - T(\mathbf{Y}, r)}{ \hat{T}(\mathbf{Y}, r)_{0.975} - T(\mathbf{Y}, r) } \right. \\ \left. + \mathbb{1}(\hat{T}(\mathbf{x}_0, r) < T(\mathbf{Y}, r)) \cdot \frac{T(\mathbf{Y}, r) - \hat{T}(\mathbf{x}_0, r)}{ \hat{T}(\mathbf{Y}, r)_{0.025} - T(\mathbf{Y}, r) } \right\}$	larger	(22), (32)
	CRPS	$\mathbb{E} \left[\int_{\mathcal{R}^*} \hat{T}(\mathbf{x}_0, r) - \hat{T}(\mathbf{Y}, r) dr \right] \\ - \frac{1}{2} \cdot \mathbb{E} \left[\int_{\mathcal{R}^*} \hat{T}(\mathbf{Y}, r) - \hat{T}(\mathbf{Y}', r) dr \right]$	larger	(25), (32)
B	INT	$\int_{\mathcal{R}^*} \hat{T}(\mathbf{x}_0, r) dr$	two-sided	(27), (32)
	POINT	$\hat{T}(\mathbf{x}_0, r^*)$	two-sided	(26), (32)
C	FUN	$\hat{T}(\mathbf{x}_0, \cdot) _{\mathcal{R}^*}$	erl	(28), (38)
	FUN	$\hat{T}(\mathbf{x}_0, \cdot) _{\mathcal{R}^*}$	area	(28), (40)
	FUN	$\hat{T}(\mathbf{x}_0, \cdot) _{\mathcal{R}^*}$	cont	(28), (37)

Table 2: Overview of the test statistics and the corresponding orderings used in the simulation study. Equations refers to the corresponding equations in Fend and Redenbach (2025) that provide the formulas for both the test statistic and the ordering. The point processes \mathbf{Y} and \mathbf{Y}' are independent and fulfill the null hypothesis, i.e. their distribution is P_0 . The quantity $\hat{T}(\mathbf{Y}, r)_\beta$ appearing in QDIR denotes the β -quantile of the distribution of $\hat{T}(\mathbf{Y}, r)$.

From the list of test statistics in Fend and Redenbach (2025), we excluded the pointwise continuous ranked probability score test statistic SCORE, as it is computationally expensive to compute both in time and in memory. In addition, some preliminary experiments showed that it did not perform better than the FUN test statistic. We also excluded the two scaled DCLF test statistics QDIR, DCLF and ST, DCLF, as prior studies recommend using the scaled MAD variants (Myllymäki et al., 2015).

3 Recommendation based on prior studies

In the literature, several power studies for goodness-of-fit tests for spatial point processes have been conducted. The common null hypothesis is complete spatial randomness. The setting of the individual studies is very diverse, but many combinations of functional summary statistic and test statistic have not yet been investigated. Nevertheless, many

interesting conclusions can already be drawn. A detailed list of all key findings from these previous power studies is given in Section 7 of Fend and Redenbach (2025). The main results are summarized in the following.

We start with the results obtained using classical functional summary statistics. For the L -function, Baddeley et al. (2014) found that the DCLF test statistics led in most cases to more powerful tests compared to the MAD statistic. By construction of the Baddeley-Silverman cell process, its theoretical K - or L -function coincides with the one from the Poisson process and thus CSR. Tests constructed with either the MAD, DCLF or INT test statistic are not able to distinguish the Baddeley-Silverman cell process from CSR. On the other hand, Heinrich-Mertsching et al. (2024) were able to detect the difference when using the CRPS statistics even when it was combined with the K -function.

The experiments in Baddeley et al. (2014) showed that the DCLF and, to some extent, the MAD test statistics are sensitive to the choice of \mathcal{R}^* . Myllymäki et al. (2017) found that FUN with the erl ordering, as well as QDIR and ST are more robust in terms of power when the upper bound r_{\max} of \mathcal{R}^* is varied.

The detailed discussion of test statistics of type A in Myllymäki et al. (2015) states that using scaling approaches like QDIR and ST or variance-stabilizing transformations of the functional summary statistic not only makes the tests more robust when varying r_{\max} but also increases their power compared to the raw version MAD. The authors conjecture that scaling alone should be sufficient in many settings.

Topological summary functions are known to yield powerful tests for the null hypothesis of CSR if the true model has complex interactions, e.g., in a Baddeley-Silverman cell process (Robins and Turner, 2016; Biscio and Møller, 2019; Biscio et al., 2020; Botnan and Hirsch, 2022). Nevertheless, Krebs and Hirsch (2022) discourage the use of a single topological summary statistics to draw conclusions, as the power greatly depends on the specific test setting. In particular, the use of 0-dimensional or 1-dimensional topological features can lead to very different decisions. An experiment in Biscio et al. (2020) investigated the combination of two topological summary statistics which increased the power. Combined tests of the classical functional summary statistics were also already considered in Mrkvička et al. (2017). Tests that combine L -, F -, G - and J -function were comparable in power to the most powerful of the individual tests.

The following concrete recommendations for the classical functional summary statistics are given in the literature:

- If the range of interaction between points in the pattern is approximately known, then one should prefer DCLF over MAD with an upper bound r_{\max} that is slightly larger than this range (Baddeley et al., 2014, 2015).
- QDIR can be recommended over ST and MAD in many settings when using classical functional summary statistics (Myllymäki et al., 2015, 2017).
- The scaled MAD test statistics are often more powerful than the scaled DCLF test statistics (Myllymäki et al., 2015).
- If extremeness is expected on a large part of \mathcal{R}^* , then one should prefer FUN with either the extreme rank length measure or the area measure. If extremeness is only expected at selected distances, then QDIR or FUN with the continuous rank measure are preferable (Mrkvička et al., 2022; Myllymäki and Mrkvička, 2020, 2024).

3.1 Open questions

Performance of topological summary statistics The recommendations above are derived from experiments with the classical functional summary statistics. In case of the topological summary statistics, it is not known whether the same recommendations can be made. In contrast to the classical summary statistics, some of the topological summary statistics are by definition integer-valued instead of real-valued which can make a difference for the tests.

Additionally, to the best of our knowledge, a proper comparison between classical and topological functional summary statistics in a common goodness-of-fit test setting has not yet been published.

Necessary number of simulations in the Monte Carlo test An important aspect in Monte Carlo testing is the number of simulations m of the null model. A discussion of this parameter can be found in Fend and Redenbach (2025, Sec. 6.5). In the literature, there are conflicting recommendations regarding the choice of m , ranging from $m = 99$ to $m = 2499$, depending on the choice of the test statistic. For some test statistics and orderings, the influence of m has not been investigated in a point process setting, and no guidelines are available.

Use of the CRPS test statistic When using the K -function, the CRPS test statistic improved the power compared to, e.g., DCLF and MAD (Heinrich-Mertsching et al., 2024). It remains open for which other summary statistics we can get a similar improvement.

Combination of topological and classical functional summary statistics Using individual topological functional summary statistics has been discouraged, while their combinations are mentioned to be worthwhile to investigate (Biscio et al., 2020). Combinations of the classical functional summary statistics led to powerful tests in Mrkvička et al. (2017). Combining both types of summary statistics in one test has not yet been considered and remains to be investigated. The knowledge about which combinations yield powerful tests then also provides more insight into in which way the topological characteristics can complement the classical probabilistic summary statistics.

4 Experimental design

We conducted several simulation studies in the case $d = 2$, i.e. planar point processes, that provide answers to the open questions outlined above.

Assume that we observe the point pattern \mathbf{x}_0 that has n distinct points in an observation window of the form $W_A = [0, \sqrt{A}]^2$ for some $A > 0$. Let P denote the true distribution of the point process model producing the realization \mathbf{x}_0 . The hypotheses are

$$H_0 : P \text{ is complete spatial randomness} \quad \text{vs.} \quad H_1 : P \text{ is not complete spatial randomness.}$$

Complete spatial randomness is modeled by the homogeneous Poisson process on \mathbb{R}^2 . This process is parametrized by the intensity $\lambda > 0$, making the hypothesis a composite hypothesis. Thus, we proceed as in Fend and Redenbach (2025, Sec. 6.1) and condition on the number of observed points in W . The null model P_0 from which we sample point patterns in the Monte Carlo test is then a binomial point process with a uniform intensity function on W . This means that we draw the x - and the y -coordinates of all n points independently and uniformly in $[0, \sqrt{A}]$.

4.1 Point process model families

In this section, the point process models used in our study are introduced. All six processes are stationary and isotropic point processes. They cover different types of processes from clustering to repulsion between points. We will introduce the models only briefly. Details can be found in Baddeley et al. (2015).

Homogeneous Poisson point process A point process \mathbf{X} on \mathbb{R}^2 is a homogeneous Poisson process with intensity $\lambda > 0$ if the number of points $\mathbf{X}(B)$ in a Borel set $B \in \mathcal{B}^2$ is Poisson distributed with rate $\lambda |B|$ and if for an arbitrary number k of disjoint Borel sets B_1, \dots, B_k we have that $\mathbf{X}(B_1), \dots, \mathbf{X}(B_k)$ are independent random variables.

Matérn cluster point process The Matérn cluster point process is an example of a process that is used to model independent clustering in circular clusters of fixed radius $R > 0$. The parents, i.e., the center points of the clusters, are given by a homogeneous Poisson process with intensity $\kappa > 0$. For each parent point, we independently draw a number of children, which is Poisson distributed with rate $\mu > 0$. We place the children independently and uniformly in the disk with radius R around the parent. Finally, the Matérn cluster point process is given as the union of the children of all parents.

Baddeley-Silverman cell process The Baddeley-Silverman cell process is constructed by dividing the space into equal area cells. For each cell the random number N_c of points within this cell is drawn independently from the discrete distribution with probability weights

$$P(N_c = 0) = \frac{1}{10}, \quad P(N_c = 1) = \frac{8}{9} \quad \text{and} \quad P(N_c = 10) = \frac{1}{90}.$$

Since $\mathbb{E}[N_c] = \text{Var}(N_c) = 1$, we use $\lfloor \lambda |W| \rfloor$ squares of equal size to obtain a process with intensity $\lambda > 0$ in an observation window W with equal side lengths. The points per cell are sampled independently and uniformly within the cell.

Hard core point process The hard core process with intensity parameter $\beta > 0$ and hard core radius $R > 0$ is a point process model in which two points are not allowed to be closer than distance R . This is realized using the density function

$$f_{\text{hardcore}}(\mathbf{x}) \propto \begin{cases} \beta^{\#\mathbf{x}} & \text{if } \min_{x_1 \neq x_2 \in \mathbf{x}} \|x_1 - x_2\| \geq R, \\ 0 & \text{else} \end{cases}$$

w.r.t. the homogeneous unit intensity Poisson process. This process can be seen as CSR under the restriction that the hard core distance is fulfilled.

Strauss point process The Strauss point process is a pairwise interaction process that is used to model repulsion between points. It is defined via the density function f_{strauss} given as

$$f_{\text{strauss}}(\mathbf{x}) \propto \beta^{\#\mathbf{x}} \prod_{x_1 \neq x_2 \in \mathbf{x}} \gamma^{\mathbb{I}(\|x_1 - x_2\| \leq R)}$$

where $\beta > 0$ is a parameter that controls the intensity, $\gamma \in [0, 1]$ gives the strength of the interaction and $R > 0$ gives the range of interaction. For $\gamma = 1$ we recover the homogeneous Poisson process and for $\gamma = 0$ and the convention $0^0 = 1$ we obtain the hard core process.

Gaussian determinantal point process Determinantal point processes (DPP) form a class of point processes which are defined using a kernel C . If the n th order product density $\rho^{(n)}$ of spatial point process \mathbf{X} on \mathbb{R}^2 is for all $n \in \mathbb{N}$ given as

$$\rho^{(n)}(z_1, \dots, z_n) = \det(C(z_i, z_j))_{1 \leq i, j \leq n} \quad \text{where } z_1, \dots, z_n \in \mathbb{R}^2,$$

then we call \mathbf{X} a (planar) DPP with kernel C . The Gaussian DPP uses the Gaussian kernel

$$C(x_1, x_2) = \lambda \cdot \exp(-\|(x_1 - x_2)/\alpha\|^2)$$

where $\lambda > 0$ is the intensity and the shape parameter α needs to fulfill $0 < \alpha < (\lambda\pi)^{-\frac{1}{2}}$ for the existence of the planar DPP (Lavancier et al., 2015).

4.2 General study parameters

Table 3 states the exact parameters that were used in this study. The parameters were chosen such that the realizations visually resemble CSR, e.g., sparse clusters for the Matérn cluster point process and a shape parameter α which is close to the largest possible one for the Gaussian DPP. We simulated each of the six point processes 1000 times on four different window sizes, namely $W_A = [0, \sqrt{A}]^2$ for $A \in \{1, 2, 6, 20\}$. Due to the intensity being set to $\lambda = 50$ we obtain patterns with approximately 50, 100, 300 and 1000 points, respectively. We used the R-package `spatstat` (Baddeley and Turner, 2005) for the simulation of all processes. One realization per model and observation window is shown in Figure 1.

Name	Point process family	Type	Parameters
Poi	homogeneous Poisson point process	complete spatial randomness	$\lambda = 50$
MatClu	Matérn cluster point process	clustered	$\kappa = 25, \mu = 2, R = 0.2$
BadSil	Baddeley-Silverman cell process	repulsive with few clusters	$\lambda = 50$
Hard	Hard core point process	hard core	$\beta = 80, R = 0.05$
Str	Strauss point process	repulsive	$\beta = 95, \gamma = 0.6, R = 1$
GDPP	Gaussian determinantal point process	repulsive	$\lambda = 50, \alpha = 0.05$

Table 3: Overview of the parameters used in the simulation study

We ran prior tests to see up to which maximal spatial distance $r_{\max} > 0$ the estimation of each functional summary statistic was possible for all six specified point process models on all four window sizes. This resulted in a maximal upper bound of $r_{\max} = 0.1$ for the distance-based summary statistics F, G and J and $r_{\max} = 0.25$ for the second-order and topological summary statistics. For all summary functions except the pcf , the relevant part of the domain \mathcal{R}^* the interval $\mathcal{R}^* = [0, r]$ for some $0 < r \leq r_{\max}$. For the pcf , we use $\mathcal{R}^* = [0.005, r]$ with some $0 < r \leq r_{\max}$ as the estimation of the pcf is unstable close to 0. For a comparison involving the point evaluation test statistic POINT, we let r^* coincide with the upper bound of \mathcal{R}^* .

We follow the default setting in `spatstat` for the estimation of the functional summary statistics and choose 513 equidistant evaluation points in each \mathcal{R}^* . The empirical topological summary statistics are implemented using the R-package TDA (Fasy et al., 2024) while we used the `spatstat` implementation of the estimators of the classical functional summary statistics.

For the DCLF and MAD tests, we used the respective `spatstat` functions while QDIR, ST and FUN with all three types of orderings are available in the R-package GET (Myllymäki and Mrkvička, 2024). Details regarding the implementation

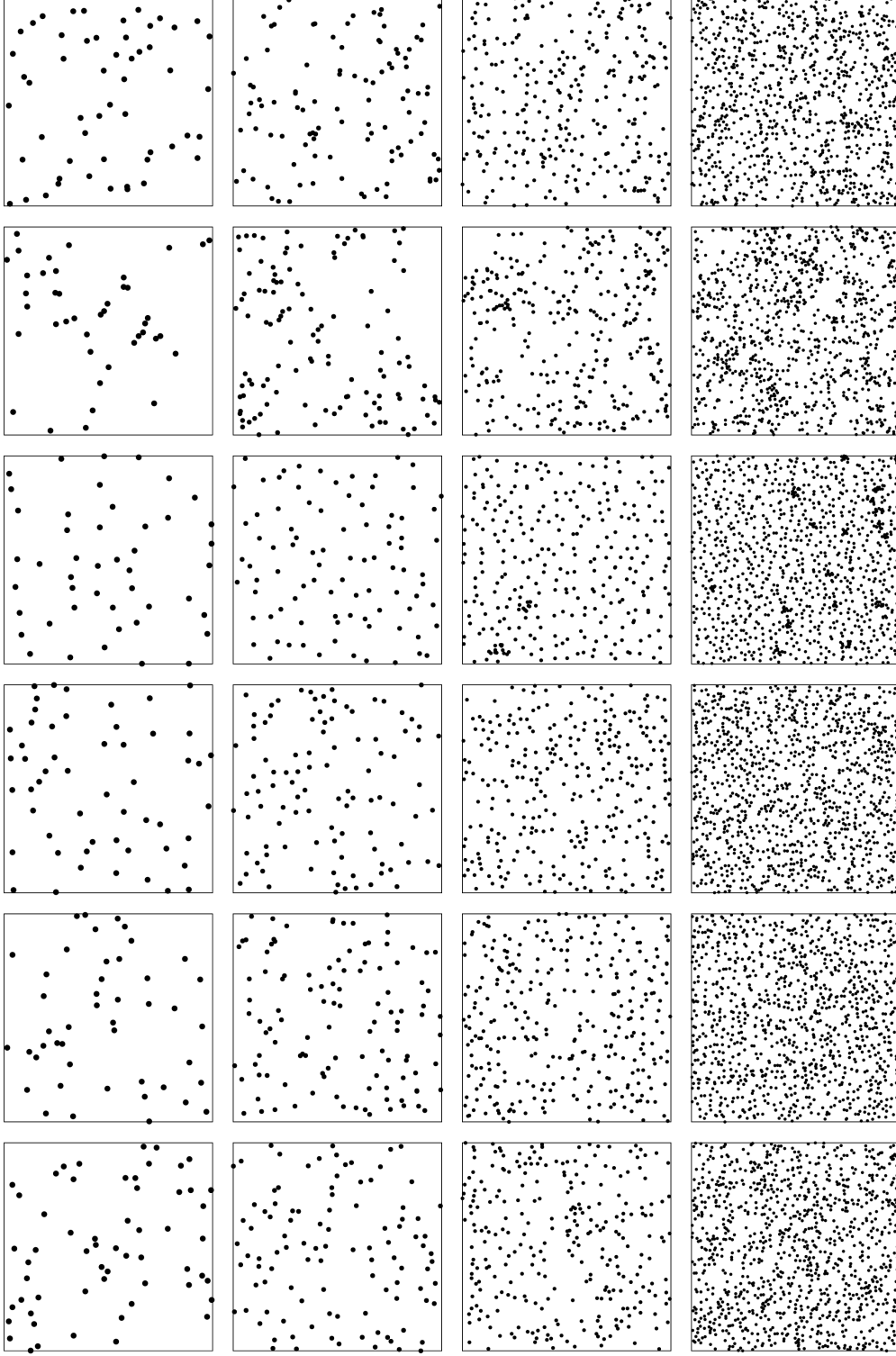


Figure 1: One realization of each of the point process models in Table 3 in each of the observation windows W_A . In the rows from top to bottom: Poi, MatClu, BadSil, Hard, Str, GDPP. In the columns from left to right: W_1 , W_2 , W_6 , W_{20} .

of the CRPS test statistic are given in Fend and Redenbach (2025). The INT test statistic is approximated using a Riemann sum.

In the Monte Carlo tests we used $m \in \{99, 299\}$ for test statistics of type A and B and $m \in \{99, 299, 499, 999\}$ for type C.

5 Results

In the following, we present a discussion of a selection of the empirical rejection rates computed for a fixed significance level of $\alpha = 0.05$. Due to the high number of tests that were conducted and thus can be compared, interactive graphics are necessary to keep the amount of information manageable. These graphics allow the reader to select the tests of interest. The interactive graphics are available in our repository <https://github.com/cfend/SpatialPointProcessesGOF>. This repository also contains the power plots for all four window sizes.

5.1 Individual functional summary statistics

In the first part of the study, we investigated the combination of a functional summary statistic and a test statistic. In the following, we show the results obtained for patterns in the observation window W_6 thus with approximately 300 points per pattern. The number of simulations is fixed to $m = 299$ unless mentioned otherwise. Examples of the empirical functional summary statistics for each model are shown in Figures 2 and 3.

Test statistics DCLF, MAD, INT and POINT

Figure 4 shows the empirical power curves for DCLF, MAD, INT and POINT in combination with the classical and topological functional summary statistics. The empirical sizes, which are not shown in the figure, met in all settings the significance level $\alpha = 0.05$.

We first discuss the results obtained for the classical functional summary statistics. For the second-order summary statistics (Figure 4 first three rows from the top) we conclude that DCLF should be preferred over MAD. The only exception is the L -function when the alternative is the GDPP, which is a repulsive point process. This agrees with the experiments in Baddeley et al. (2014). The pure integral test statistic INT often results in higher empirical powers, especially for the pcf and the K -function. But, as expected, due to the high variability in the estimation of the K -function the tests are less robust with respect to the upper bound. The L -function or the pcf should be preferred in all cases. The test statistic POINT cannot be recommended for the pcf. For the other two second-order characteristics K and L , POINT should only be used if a clear interaction distance is known a priori as the range with high power is considerably smaller than for the other three test statistics. For r_{\max} larger than this interaction distance, POINT is not able to distinguish the alternatives from CSR. All these observations agree with the general recommendations of Baddeley et al. (2014, 2015) that the upper bound should be chosen slightly larger than the interaction distance of the point process when using second-order characteristics.

For the remaining three classical summary statistics F , G and J , MAD is often slightly more powerful than DCLF and INT, but also more sensitive to the choice of the upper bound r_{\max} . The same conclusion can also be drawn for the other three observation windows with the results being available in the online repository. The POINT evaluation test statistic is powerful and competitive in combination with F , G and J . In most cases, the power is similar to that of the MAD test statistic, with the same drawback of the sensitivity w.r.t. the choice of the specific evaluation point, which is chosen as the upper bound r_{\max} of the interval used for MAD.

For the topological summary statistics in Figure 4 we can observe that the DCLF test statistic always yields more powerful tests compared to the MAD test statistic for the null hypothesis of CSR. The INT test statistic can be very powerful and even outperform DCLF but the power depends extremely on the upper bound r_{\max} . The dependence on r_{\max} is even more severe for the POINT test statistic. For the three integer-valued summary statistics β_0 , β_1 and χ , the power fluctuates a lot, and we obtain competitive tests only at a few selected distances. The use of POINT with these topological summary statistics is therefore discouraged. For the two cumulative and hence real-valued functions APF_0 and APF_1 , POINT behaves similarly to MAD while also picking up the fluctuations of the INT test statistic.

Except for β_0 , we notice a clear drop in power at some distances when using the topological summary statistics with DCLF, MAD and INT. This can be explained by comparing the pointwise means and variances of the functional summary statistics shown in Figure 3. The 1-dimensional Betti curves of the five alternative models differ the most from the one of the Poi null model in the location and shape of the peak. Thus, the tests are most powerful when they use the entire information available up to the peak. Similar to the second-order characteristics, the power drops slightly when choosing an upper bound that is even larger than the distance at which the peak occurs. For the two accumulated

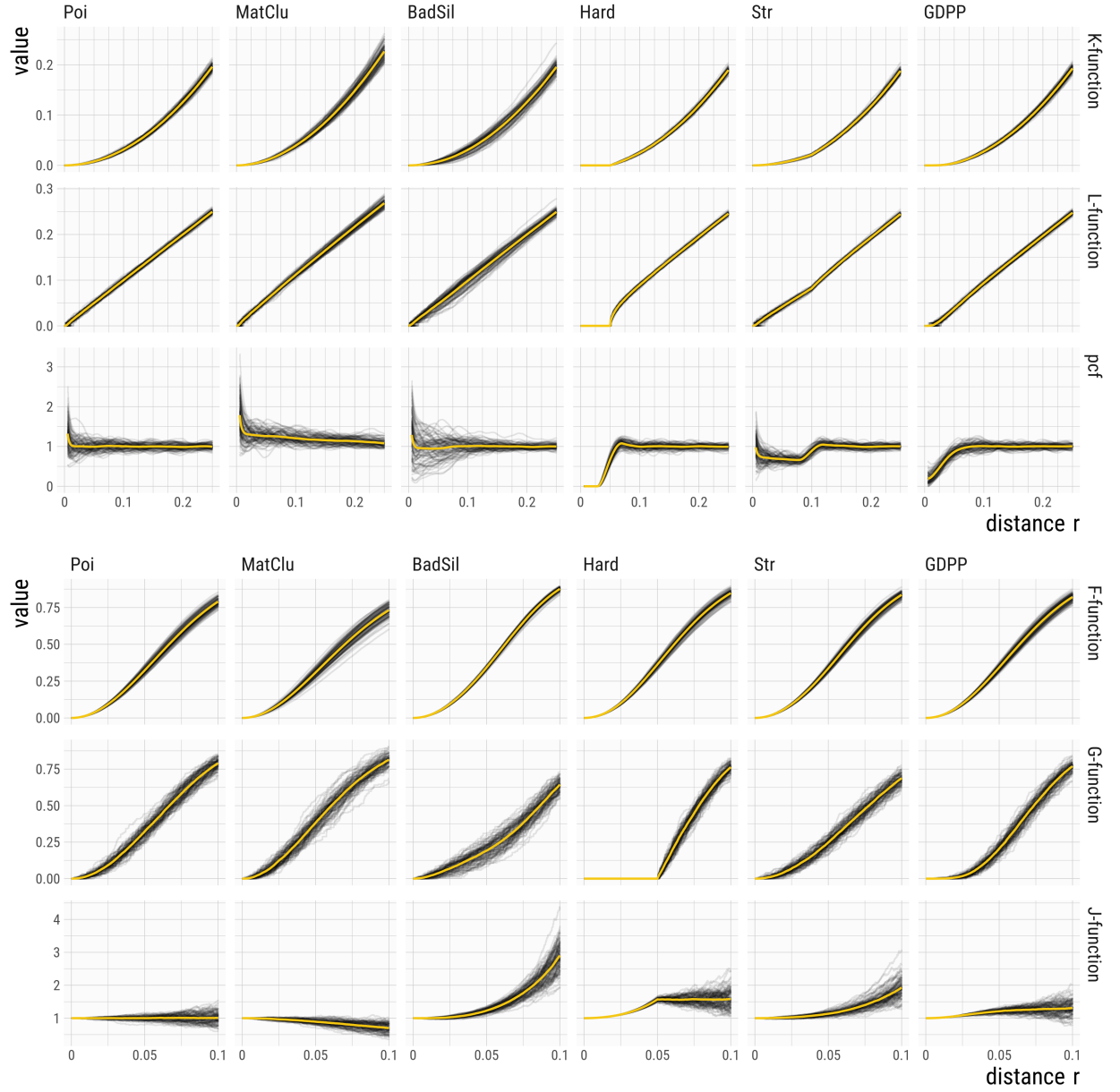


Figure 2: Empirical classical functional summary statistics from 100 realizations per model on window W_6 . In yellow the pointwise mean of the individual estimates.

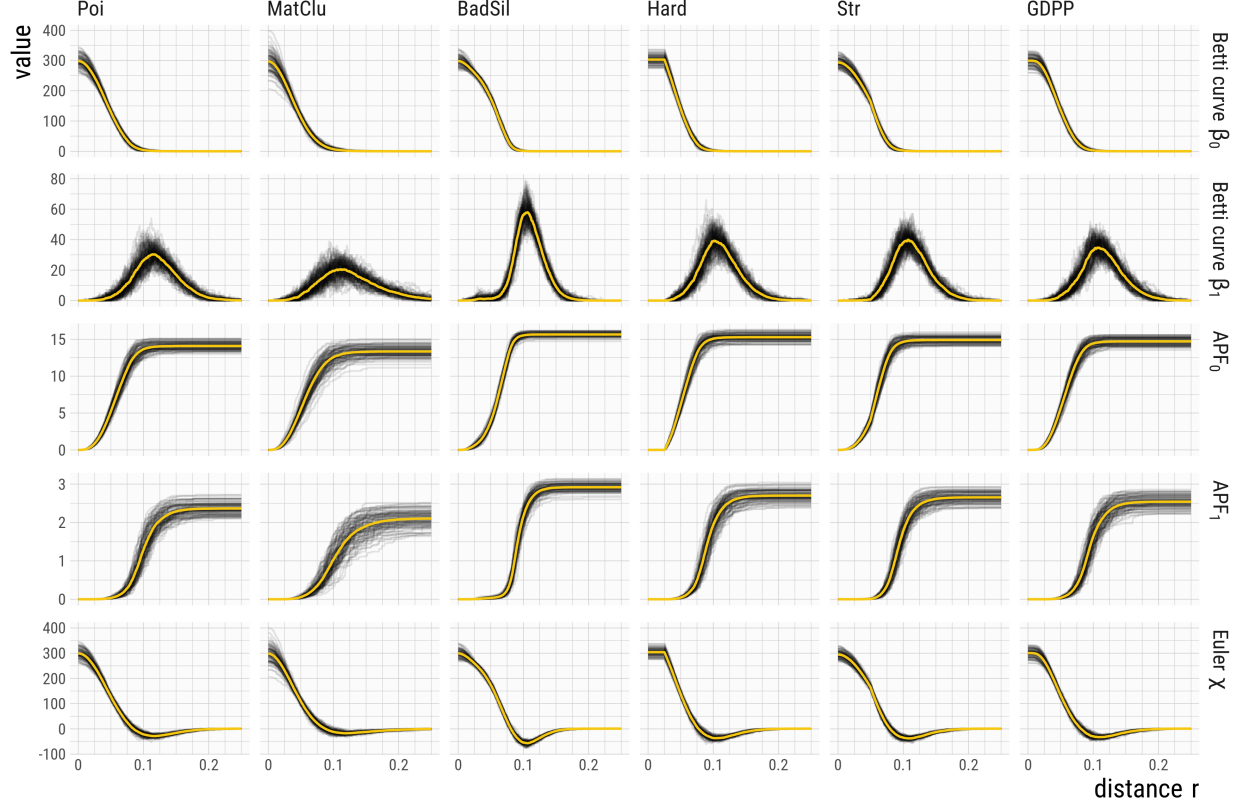


Figure 3: Empirical topological functional summary statistics from 100 realizations per model on window W_6 . In yellow the pointwise mean of the individual estimates.

persistence functions, we notice large pointwise variances under the null model. The curves from different models overlap and cross each other, leading to decreases in power, in particular when using the INT test statistic. In general, we recommend using the largest possible upper bound for these two functional summary statistics in order to take the entire persistent homology information into account. The Euler characteristic χ is the most powerful at small distances, where almost no 1-dimensional features exist. The characteristic is negative if there are more 1-dimensional than 0-dimensional features, which is the case around the peak of β_1 . Hence, the power with INT decreases at the distance where β_1 with INT is the most powerful. Increasing the upper bound for χ does not recover the highest power for all models since all curves eventually converge to the same value of 1. Consequently, using INT with χ is discouraged and we recommend using DCLF instead.

In general, for testing CSR, topological summary statistics using 0-dimensional features (β_0 , APF_0 , χ) are more powerful than the 1-dimensional ones. The 1-dimensional characteristics that consider circular “holes” typically require longer distances to be able to discriminate between CSR and any dependence between the points.

Test statistics QDIR, ST and FUN

The empirical power curves for the FUN test statistic with the three types of ordering and the scaled MAD test statistics ST and QDIR are shown in Figure 5.

Consider first the FUN test statistic with the three types of ordering. For all five models and the classical second-order summary statistics K , L and pcf as well as G and J , we obtain almost the same empirical rejection rates for all three orderings. For the empty space function F , the cont ordering yields less powerful tests than the other two orderings.

For the topological summary statistics, the difference between the three orderings becomes clearer. In particular, erl gives the most powerful tests, followed by $area$ and then $cont$. The continuous rank ordering performs considerably

worse than the other two if used with the 1-dimensional Betti curve β_1 . We provide in Appendix A an illustrative example that shows why the cont ordering is not a good choice for this specific summary statistic.

Overall in the setting of testing CSR, the erl ordering can be recommended for all the considered functional summary statistics.

Next, we concentrate on the two scaling approaches, ST and QDIR. The figure clearly shows that QDIR is significantly more powerful than ST. The only exception is the pair correlation function, where the choice between the five test statistics has no influence, and the purely 1-dimensional topological statistics β_1 and APF_1 where both scaling approaches do not work at all.

In case of the topological summary statistics, recall that β_0 , β_1 and χ are integer-valued. At each evaluation point, we have a highly discrete distribution of a small number of possible values. Thus the denominators of the test statistics ST and QDIR given as the empirical standard deviation and the absolute difference between an empirical quantile and the sample mean, respectively, can be very small. This results in very large test statistics even for the simulations of the null model. Consequently the tests are less powerful. The problem is especially severe for β_1 at small distances. The accumulated persistence functions, in particular APF_1 , inherit the problem of having only few possible values from the corresponding Betti numbers.

Functional summary statistic T	upper bound r_{\max}									
	0.01	0.025	0.05	0.075	0.1	0.125	0.15	0.175	0.2	0.25
β_0	0.052	0.053	0.057	0.052	0.059	0.048	0.049	0.056	0.062	0.058
β_1	0.036	0.041	0.046	0.038	0.038	0.037	0.035	0.032	0.036	0.037
APF_0	0.052	0.053	0.060	0.050	0.060	0.052	0.058	0.058	0.058	0.062
APF_1	0.039	0.051	0.056	0.051	0.048	0.050	0.054	0.052	0.049	0.051
χ	0.051	0.058	0.063	0.060	0.062	0.060	0.057	0.067	0.065	0.042

Table 4: Empirical rejection rates for the nominal level $\alpha = 0.05$ for the test with test statistic QDIR obtained for the CSR-model Poi from 1000 realizations on W_6 . Highlighted in bold are the empirical rates where the approximated 0.95-CI for the true p -value does not contain the nominal level.

The problem of combining topological summary statistics with scaling approaches is also illustrated in the empirical sizes of the tests obtained with QDIR, which are listed in Table 4. The tests with QDIR and β_1 are conservative based on the results obtained from 1000 replications of the test. The empirical sizes of ST are similar.

From all results shown in Figure 5 it is clear that when using the same number of realizations m , the FUN test statistic should be preferred over the scaling approaches. Not only does it provide more powerful tests than QDIR, but it is also more robust with respect to the upper bound r_{\max} .

Test statistic CRPS

Finally, we compare DCLF, FUN with erl and the recently introduced CRPS test statistic. The corresponding power curves are shown in Figure 6.

Overall, the DCLF and CRPS test statistics result in tests with comparable power for most functional summary statistics. This makes sense due to the construction as both consider in some sense the squared deviation to the null model. In cases where the variability of the functional summary statistics under the null model is high, CRPS is more powerful. For example, this is the case for the K - and J -function at larger distances, the pair correlation function, and the 1-dimensional topological characteristics β_1 and APF_1 .

Compared with the two deviation-based test statistics DCLF and CRPS, FUN with erl results in more robust tests with respect to the varying upper bound r_{\max} not only for the classical summary statistics, but also for the topological ones. As mentioned above, the drop in power for β_1 and APF_1 with deviation-based test statistics is noticeable for most alternatives and appears even on the largest window W_{20} with about 1000 points. With FUN and the erl ordering, we do not observe any drop.

When considering the absolute power for alternatives that exhibit clustering as MatClu, we can conclude that deviation-based test statistics are more powerful than FUN. For the repulsive GDPP model, the FUN test statistic with erl ordering

is more powerful than DCLF and CRPS for all functional summary statistics except for the purely 1-dimensional topological summary statistics β_1 and APF_1 .

Number of simulations m

The remaining open question regarding Monte Carlo tests with a single functional summary statistic is the number of simulations m . So far, we discussed the results obtained using $m = 299$ for all test statistics. Although this choice is larger than the numbers often used for the deviation-based test statistics of type A in the literature, it is smaller than recommendations for the FUN test statistic.

Figure 7 displays the rejection rate curves obtained for the FUN test statistic with either the *erl* or the *cont* ordering for different choices of the number of simulations m . As discussed previously, the continuous rank measure is less powerful than *erl* in our setting. We can also see that *cont* with $m = 999$ is often still less powerful than *erl* with $m = 99$ simulations, while being computationally much more expensive. The only big increase of power due to a higher number of simulations can be observed when going from $m = 99$ to $m = 299$ in case of the *cont* measure. This happens both for the classical and the topological functional summary statistics.

Due to the aforementioned problems with the 1-dimensional topological features, *cont* benefits from a higher number of simulations for that specific summary statistics. Hence, only for β_1 and APF_1 an ongoing increase in power is visible. There are only minor differences for the *erl* ordering in our study. It should be noted that for several functional summary statistics either $m = 99$ or $m = 299$ yields the most powerful test, and with $m = 999$ the power was considerably lower. Based on this simulation study, there is no evidence to recommend a higher number than $m = 299$ for the simulations when using the FUN test statistic with *erl* ordering.

As mentioned in Fend and Redenbach (2025), many authors use $m = 99$ for MAD or DCLF. In our results shown in Figure 8 the power curves for DCLF and INT for $m = 299$ are compared with those obtained when using $m = 99$. Overall, the differences are rather small on the observation window W_6 . On the two smaller observation windows, the increase from using $m = 299$ is larger and thus if it is computationally feasible we recommend $m = 299$ for test statistics of type A and B.

5.2 Combination of several functional summary statistics

We compared tests that use a single summary statistic with similar tests that combine several of them. From the results obtained in the previous experiments, we selected the L -function as best second-order characteristic, the J -function representing the distance-based summaries, and the 0-dimensional Betti curve and the Euler characteristic curve as topological summary statistics. We selected two topological summary functions as β_0 only takes the information on the 0-dimensional topological features into account while χ also includes the 1-dimensional features. For the comparison we used the FUN test statistic with the *erl* ordering where we discretized each functional summary statistic at 513 equidistant evaluation points. In all tests, we used $m = 299$ simulations from CSR. The combined tests were conducted using the two-step combination procedure available in the GET-function `global_envelope_test` (Myllymäki and Mrkvička, 2024).

The L -function was estimated on the interval $[0, 0.25]$, the J -function on $[0, 0.1]$, the 0-dimensional Betti curve β_0 on $[0, 0.1]$ and the Euler characteristic curve χ on $[0, 0.25]$. The selected upper bounds were chosen as those that result in the highest overall powers for the individual summary functions. Note that this choice is not necessarily optimal for all of the non-CSR point process models. As an example, the Euler characteristic curve χ is more powerful against a GDPP alternative at very small distances up to 0.03.

In Table 5 the empirical power estimates for the compared tests are listed. The empirical rejection rates for the CSR-model Poi were in all cases close to the nominal level of $\alpha = 0.05$.

From the estimates, we can conclude that the combined tests are often similar in power to the most powerful individual test. This aligns with the results in Mrkvička et al. (2017) regarding combinations of the classical summary functions.

When used individually, the topological summary functions are rarely more powerful than the classical summary functions. But in combination with either of the two classical summary functions, we obtain tests that can be even more powerful than combining L and J . This is, for example, the case for the Baddeley-Silverman cell process on the two smaller windows. A combination of at least one of the classical summary functions with a topological one led to a power that is higher than the individual powers and higher than the combination of L and J . Another example is the combination of χ and L for the clustered alternative MatClu. For more regular alternatives, β_0 and J turned out to be a powerful combination in our experiments.

	Model	L	J	β_0	χ	β_0, L	χ, L	β_0, J	χ, J	J, L	χ, β_0	β_0, J, L
W_1 (50 points)	MatClu	0.274	0.122	0.158	0.181	0.256	0.288	0.144	0.173	0.278	0.193	0.270
	BadSil	0.746	0.592	0.645	0.653	0.790	0.775	0.690	0.673	0.807	0.645	0.822
	Hard	0.902	0.968	0.948	0.871	0.899	0.809	0.956	0.945	0.945	0.928	0.944
	Str	0.332	0.216	0.277	0.248	0.286	0.270	0.295	0.242	0.295	0.253	0.290
	GDPP	0.168	0.269	0.178	0.122	0.140	0.121	0.222	0.221	0.232	0.140	0.196
W_2 (100 points)	MatClu	0.535	0.198	0.298	0.375	0.527	0.546	0.286	0.342	0.514	0.366	0.504
	BadSil	0.550	0.924	0.960	0.966	0.978	0.974	0.982	0.977	0.961	0.965	0.986
	Hard	1.000	1.000	1.000	1.000	1.000	0.999	1.000	1.000	1.000	1.000	1.000
	Str	0.683	0.454	0.568	0.523	0.642	0.627	0.563	0.521	0.646	0.532	0.607
	GDPP	0.406	0.566	0.426	0.349	0.350	0.321	0.505	0.476	0.483	0.367	0.433
W_6 (300 points)	MatClu	0.951	0.519	0.679	0.809	0.944	0.944	0.649	0.782	0.944	0.785	0.936
	BadSil	0.530	1.000	1.000	1.000	1.000	1.000	1.000	1.000	1.000	1.000	1.000
	Hard	1.000	1.000	1.000	1.000	1.000	1.000	1.000	1.000	1.000	1.000	1.000
	Str	0.998	0.955	0.986	0.985	0.997	0.998	0.987	0.985	0.997	0.985	0.993
	GDPP	0.977	0.993	0.984	0.964	0.959	0.957	0.987	0.987	0.985	0.969	0.981
W_{20} (1000 points)	MatClu	1.000	0.982	0.996	1.000	1.000	1.000	0.994	1.000	1.000	0.999	1.000
	BadSil	0.546	1.000	1.000	1.000	1.000	1.000	1.000	1.000	1.000	1.000	1.000
	Hard	1.000	1.000	1.000	1.000	1.000	1.000	1.000	1.000	1.000	1.000	1.000
	Str	1.000	1.000	1.000	1.000	1.000	1.000	1.000	1.000	1.000	1.000	1.000
	GDPP	1.000	1.000	1.000	1.000	1.000	1.000	1.000	1.000	1.000	1.000	1.000

Table 5: Empirical power estimates from 1000 realizations when using the test statistic FUN and the ordering erl. The function parameters are stated in the text. For each row, the bold values indicate the highest power from a single summary function and from a combination. Rows with more than two perfect rejection rates of 1.000 per type (single or combination) are not printed in bold face.

The empirical power of the combination of the three functions β_0 , J and L is, except for the Baddeley-Silverman cell process, often slightly smaller than the power for a combination of two summary functions. In these cases, adding the third type of information is not beneficial.

6 Discussion

The focus of this study was on comparing the performance of classical and topological functional summary statistics in a common goodness-of-fit testing scenario. Our common test setting is the null hypothesis of complete spatial randomness of a planar point process with five stationary and isotropic alternatives that deviate from CSR in different ways. We investigated the empirical sizes and powers of a diverse set of tests. In particular different constructions for the test statistic as well as different orderings for vector-valued test statistics were included. Several tuning parameters such as the number of simulations in the Monte Carlo test and the relevant part of the domain of the functional summary statistic affect the performance of the test. This is the reason why we investigated their influence to see which of the tests are more robust when these parameters are adapted. With many possible parameters taken into account, we obtained

Test Statistic D	Functional Summary Statistic T										
	Second order			Distance-based			TDA-based				
	K	L	pcf	F	G	J	β_0	β_1	APF_0	APF_1	χ
Type A											
MAD	(✓)	(✓)	✗	✓*	✓	✓	✓	✗	✗	✗	✗
DCLF	(✓)	✓*	✓	✓	✓*	✓	✓*	✓	✓	✓	✓*
QDIR	✓	(✓)	✓	✗	✗	✗	✗	✗	✗	✗	✗
ST	✗	✗	✓	✗	✗	✗	✗	✗	✗	✗	✗
CRPS	(✓)	✓	✓*	✓	✓	✓*	✓	✓*	✓	✓*	✓
Type B											
INT	(✓)	✓	✓*	✓	✓	✓	(✓)	✓	(✓)	(✓)	✗
POINT	✗	✗	✗	✓	(✓)	(✓)	✗	✗	✓	✓	✗
Type C											
FUN with	erl	✓*	✓*	✓	✓	✓*	✓*	✓*	✓	✓*	✓*
	area	✓	✓	✓	✓	✓	✓	(✓)	(✓)	(✓)	✓
	cont	✓	✓	✓	✗	✓	✓	✗	(✓)	✗	(✓)

Table 6: General recommendations derived from our power study regarding which functional summary statistic should be used with which test statistic. Here we assume $m = 299$ for all tests. Recommended combinations are indicated by ✓, combinations which one should avoid by ✗. In case we can recommend a test only with certain restrictions – e.g. due to a high sensitivity w.r.t. the choice of upper bound r_{\max} or due to it being slightly less powerful than another test statistic – the symbol (✓) is used. For each functional summary statistic, i.e. each column, the symbol ✓* is used for the overall most powerful test statistics.

a large number of distinct specific tests that were conducted. Additionally, we considered four different sizes for the observation window. The results for W_6 with approximately 300 points per point pattern are shown in Figures 4 to 8 and the results for W_1 , W_2 and W_{20} are available in our online repository.

The overall performance of the combination of functional summary statistic on one hand and the test statistic and ordering on the other hand is summarized in Table 6. In particular, the test statistics DCLF, CRPS and FUN with the erl ordering performed well no matter the chosen functional summary statistics. For most of the other statistics, the performance is very sensitive with respect to the tuning parameters, in particular the choice of the upper bound r_{\max} . Whether we can recommend such a test statistic for a specific summary function depends on how straight-forward it is to select these additional parameters. For some of the functional summary statistics, the *best* test statistics depends on the type of alternative. In particular, the order of the test statistics in terms of empirical power is sometimes inverted between the clustered MatClu model and the repulsive GDPP model. In these cases, we based our recommendations on the order obtained for the majority of the alternatives.

In Section 3.1 we formulated four open questions regarding goodness-of-fit testing for spatial point processes, which we are now able to answer.

The first topic addresses the performance of topological summary statistics. In contrast to the classical functional summary statistics, in particular the second-order characteristics, only selected test statistics can be recommended. For the topological summary statistics both scaling approaches QDIR and ST as well as the cont ordering perform worse than DCLF, CRPS or FUN with the erl ordering. The difference between the test statistics is the largest for the 1-dimensional topological features, where at small distances only few holes with short lifetimes exist. This results in highly discrete pointwise distributions of the value of the functional summary statistic. The existence of such a single

small hole – that could also be considered topological noise – can change the test decision. Besides this, the Euler characteristic is also special, since it is the only functional summary statistic in our selection that can become negative before eventually converging to a limiting value of 1 for increasing spatial distance. Consequently, test statistics that take absolute differences into account should be preferred for χ and the raw INT test statistic is less discriminatory.

The second open question asked for the necessary number of simulations m . Based on our experiments (with results shown in Figures 7 and 8) we can conclude that $m = 99$ is a reasonable choice for the scalar-valued test statistics of type A (except QDIR and ST) and B . The improvement obtained from $m = 299$ is more pronounced the fewer points there are in the point pattern. For the FUN test statistic $m = 99$ is not enough. With the erl and area orderings, $m = 299$ results in powerful tests. Any further increase sometimes even decreased the empirical power. In contrast to that, we need a higher number of simulation for the cont ordering. In many cases, even $m = 999$ for cont was not as powerful as the erl ordering with $m = 299$. In prior works (e.g. Mrkvička et al., 2017) it is stated that the scaled MAD test statistics QDIR and ST require fewer simulations than FUN with the erl ordering. In our results, QDIR and ST were rarely competitive even when using the same number of simulations.

The use of the CRPS test statistics was the third open question. By construction, DCLF and CRPS behave very similarly. We recommend CRPS over DCLF in cases where the functional summary statistic estimator has a high and non-constant pointwise variance as it resulted in more powerful tests. This is the case for the K -function, the pcf and the 1-dimensional topological characteristics β_1 and APF_1 . If DCLF and CRPS are equally powerful, we recommend taking DCLF as CRPS is computationally more expensive.

Our last open question considered combinations of topological and classical functional summary statistics. Based on the results in Section 5.2 we conclude that the L -function and the Euler characteristic χ as well as β_0 and the J -function, complement each other well. The first pair is powerful in detecting clustering, whereas the second pair performs well for strongly repulsive processes. The combined tests of classical and topological summary statistics are similar or even more powerful than the individual tests, which is in agreement with the results in Mrkvička et al. (2022) obtained for combinations of the classical functional summary statistics.

In this work, we restricted ourselves to the Monte Carlo test setting. For several of the combinations, limit theorems under the CSR assumption are also available. Thus, it is still an interesting question to see how large the point pattern needs to be such that a derived asymptotic test is reasonable and powerful. Although our results provide guidelines on how to choose the test statistic and the other tuning parameters once a specific functional summary statistic has been chosen, we did not discuss how to choose the summary statistic itself. This choice in general depends a lot on the alternatives that one considers. If in doubt, the results for combined tests show that combining classical and topological functional summary statistics can yield very powerful tests that detect several different deviations from the null hypothesis. Thus, it is worthwhile to investigate these combinations in even more depth.

References

- A. Baddeley and R. Turner. spatstat: An R package for analyzing spatial point patterns. *Journal of Statistical Software*, 12(6):1–42, 2005. doi:10.18637/jss.v012.i06.
- A. Baddeley, P. J. Diggle, A. Hardegen, T. Lawrence, R. K. Milne, and G. Nair. On tests of spatial pattern based on simulation envelopes. *Ecological Monographs*, 84(3):477–489, 2014. doi:10.1890/13-2042.1.
- A. Baddeley, E. Rubak, and R. Turner. *Spatial Point Patterns: Methodology and Applications with R*. Chapman and Hall/CRC Press, London, 2015. ISBN 9781482210200. URL <https://www.routledge.com/Spatial-Point-Patterns-Methodology-and-Applications-with-R/Baddeley-Rubak-Turner/p/book/9781482210200/>.
- C. A. N. Biscio and J. Møller. The accumulated persistence function, a new useful functional summary statistic for topological data analysis, with a view to brain artery trees and spatial point process applications. *Journal of Computational and Graphical Statistics*, 28(3):671–681, 2019. doi:10.1080/10618600.2019.1573686.
- C. A. N. Biscio, N. Chenavier, C. Hirsch, and A. M. Svane. Testing goodness of fit for point processes via topological data analysis. *Electronic Journal of Statistics*, 14(1):1024–1074, 2020. doi:10.1214/20-EJS1683.
- M. B. Botnan and C. Hirsch. On the consistency and asymptotic normality of multiparameter persistent Betti numbers. *Journal of Applied and Computational Topology*, 2022. ISSN 2367-1734. doi:10.1007/s41468-022-00110-9.
- N. A. C. Cressie. *Statistics for Spatial Data*. Probability & Mathematical Statistics S. John Wiley & Sons, 2 edition, 1993.
- P. J. Diggle. On parameter estimation and goodness-of-fit testing for spatial point patterns. *Biometrics*, 35(1):87–101, 1979. ISSN 0006-341X. doi:10.2307/2529938.

- B. T. Fasy, J. Kim, F. Lecci, C. Maria, D. L. Millman, and V. Rouvreau. *TDA: Statistical Tools for Topological Data Analysis*, 2024. URL <https://CRAN.R-project.org/package=TDA>. R package version 1.9.1.
- C. Fend and C. Redenbach. Goodness-of-fit tests for spatial point processes: A review, 2025. URL <https://arxiv.org/abs/2501.03732>.
- C. Heinrich-Mertsching, T. L. Thorarinsdottir, P. Guttorp, and M. Schneider. Validation of point process predictions with proper scoring rules. *Scandinavian Journal of Statistics*, 51(4):1533–1566, 2024. doi:10.1111/sjos.12736.
- J. Krebs and C. Hirsch. Functional central limit theorems for persistent Betti numbers on cylindrical networks. *Scandinavian Journal of Statistics*, 49(1):427–454, 2022. ISSN 1467-9469. doi:10.1111/sjos.12524.
- F. Lavancier, J. Møller, and E. Rubak. Determinantal point process models and statistical inference. *Journal of the Royal Statistical Society Series B: Statistical Methodology*, 77(4):853–877, 2015. ISSN 1369-7412. doi:10.1111/rssb.12096. URL <https://doi.org/10.1111/rssb.12096>.
- N. B. Loosmore and E. D. Ford. Statistical inference using the G or K point pattern spatial statistics. *Ecology*, 87(8):1925–1931, 2006. doi:10/bgpbg.
- J. Møller and R. P. Waagepetersen. *Statistical Inference and Simulation for Spatial Point Processes*. CRC Press, 2003. ISBN 978-0-203-49693-0.
- T. Mrkvička, M. Myllymäki, and U. Hahn. Multiple Monte Carlo testing, with applications in spatial point processes. *Statistics and Computing*, 27(5):1239–1255, 2017. ISSN 1573-1375. doi:10.1007/s11222-016-9683-9.
- T. Mrkvička, M. Myllymäki, M. Kuronen, and N. N. Narisetty. New methods for multiple testing in permutation inference for the general linear model. *Statistics in Medicine*, 41(2):276–297, 2022. ISSN 1097-0258. doi:10.1002/sim.9236.
- M. Myllymäki and T. Mrkvička. Comparison of non-parametric global envelopes, 2020. URL <https://arxiv.org/abs/2008.09650>.
- M. Myllymäki and T. Mrkvička. GET: Global Envelopes in R. *Journal of Statistical Software*, 111:1–40, 2024. ISSN 1548-7660. doi:10.18637/jss.v111.i03.
- M. Myllymäki, P. Grabarnik, H. Seijo, and D. Stoyan. Deviation test construction and power comparison for marked spatial point patterns. *Spatial Statistics*, 11:19–34, 2015. ISSN 2211-6753. doi:<https://doi.org/10.1016/j.spasta.2014.11.004>.
- M. Myllymäki, T. Mrkvička, P. Grabarnik, H. Seijo, and U. Hahn. Global envelope tests for spatial processes. *Journal of the Royal Statistical Society: Series B (Statistical Methodology)*, 79(2):381–404, 2017. doi:10.1111/rssb.12172.
- B. D. Ripley. Modelling spatial patterns. *Journal of the Royal Statistical Society: Series B (Methodological)*, 39(2):172–192, 1977. ISSN 2517-6161. doi:10.1111/j.2517-6161.1977.tb01615.x.
- V. Robins and K. Turner. Principal component analysis of persistent homology rank functions with case studies of spatial point patterns, sphere packing and colloids. *Physica D: Nonlinear Phenomena*, 334:99–117, 2016. ISSN 0167-2789. doi:10.1016/j.physd.2016.03.007.

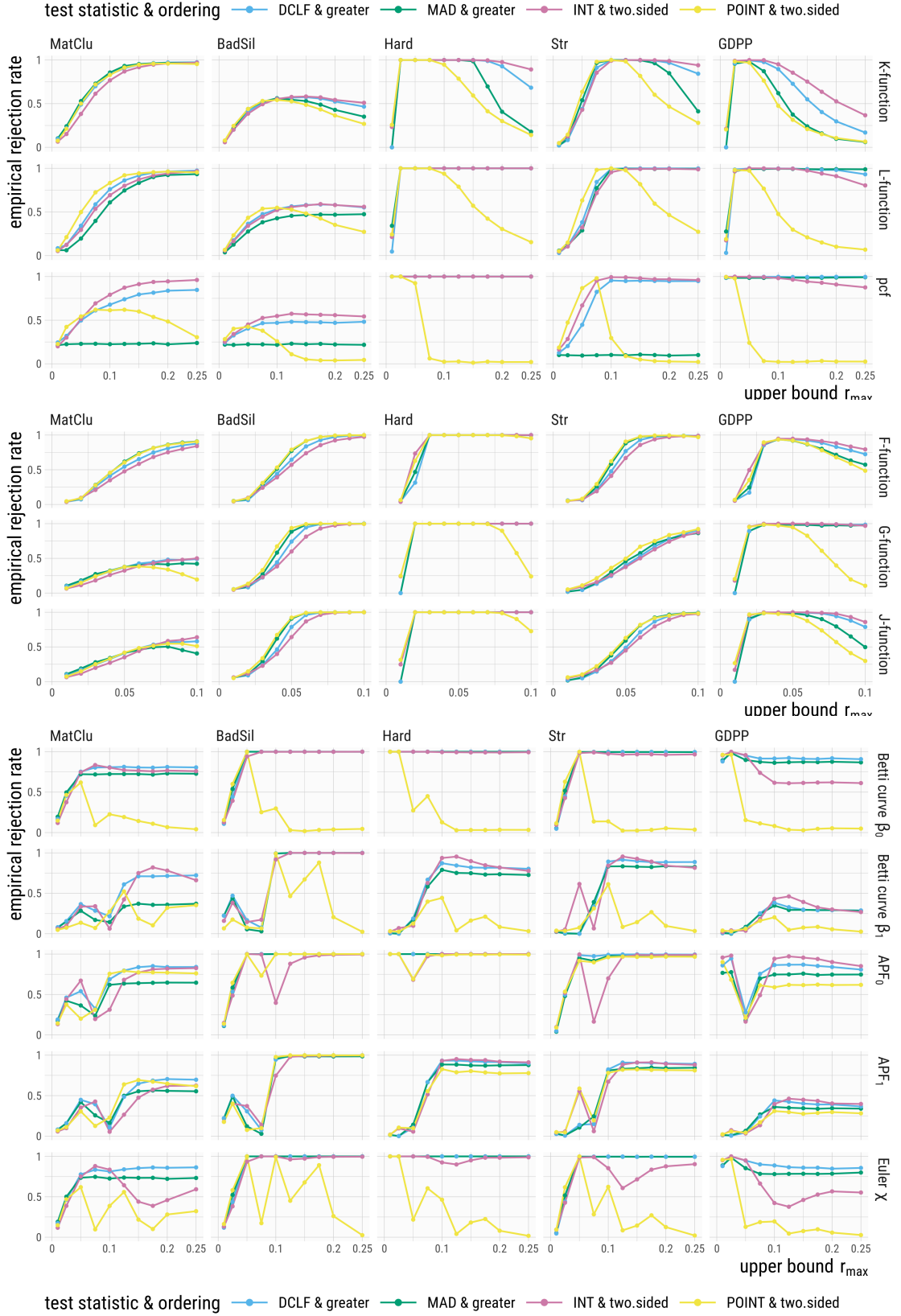


Figure 4: Empirical power curves for the test statistics DCLF, MAD, INT and POINT with respect to the upper bound r_{\max} of the domain \mathcal{R}^* . We used $m = 299$ simulations on the observation window W_6 .

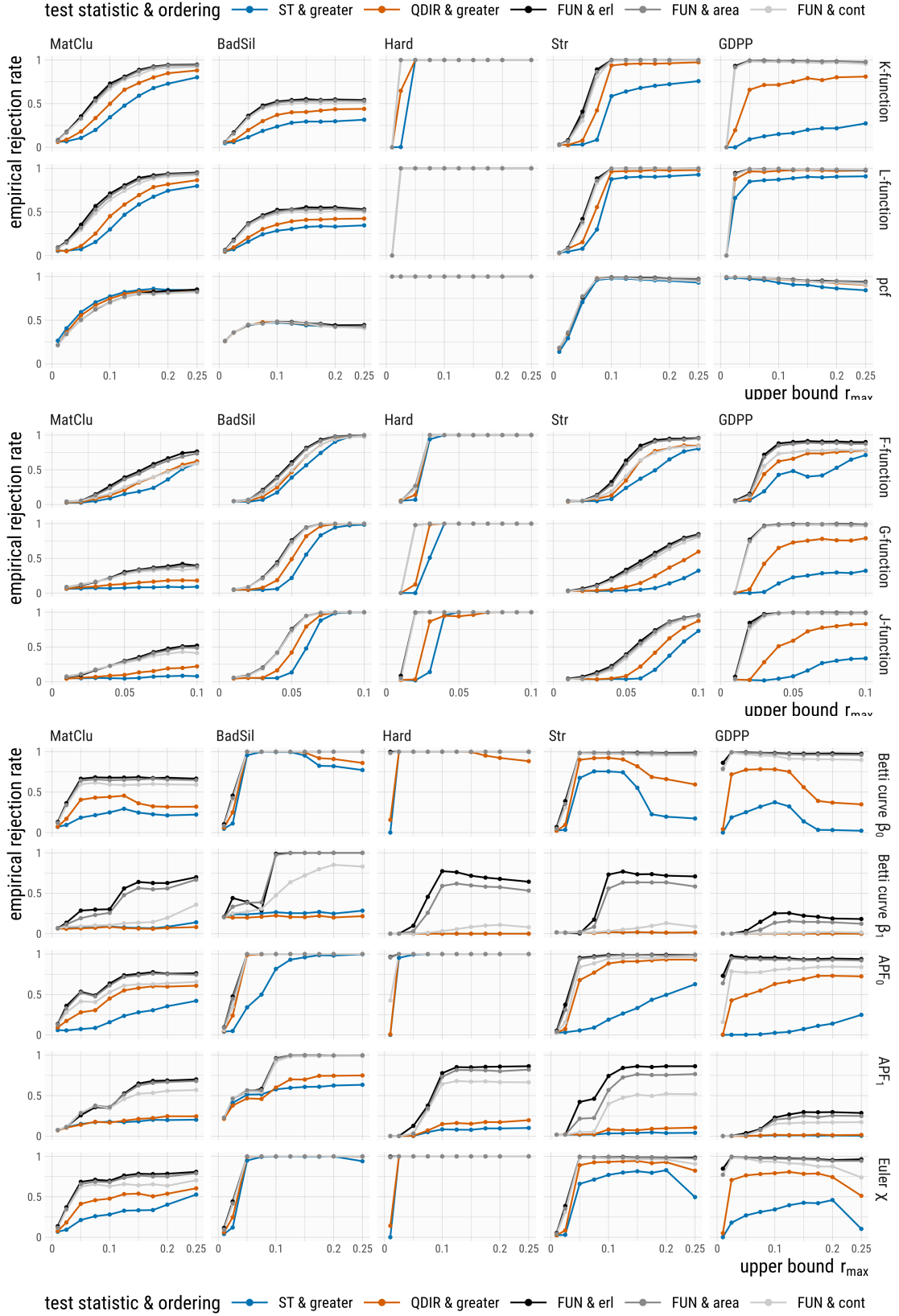


Figure 5: Empirical power curves for the test statistics ST, QDIR and FUN with respect to the upper bound r_{\max} of the domain \mathcal{R}^* . We used $m = 299$ simulations on the observation window W_6 .

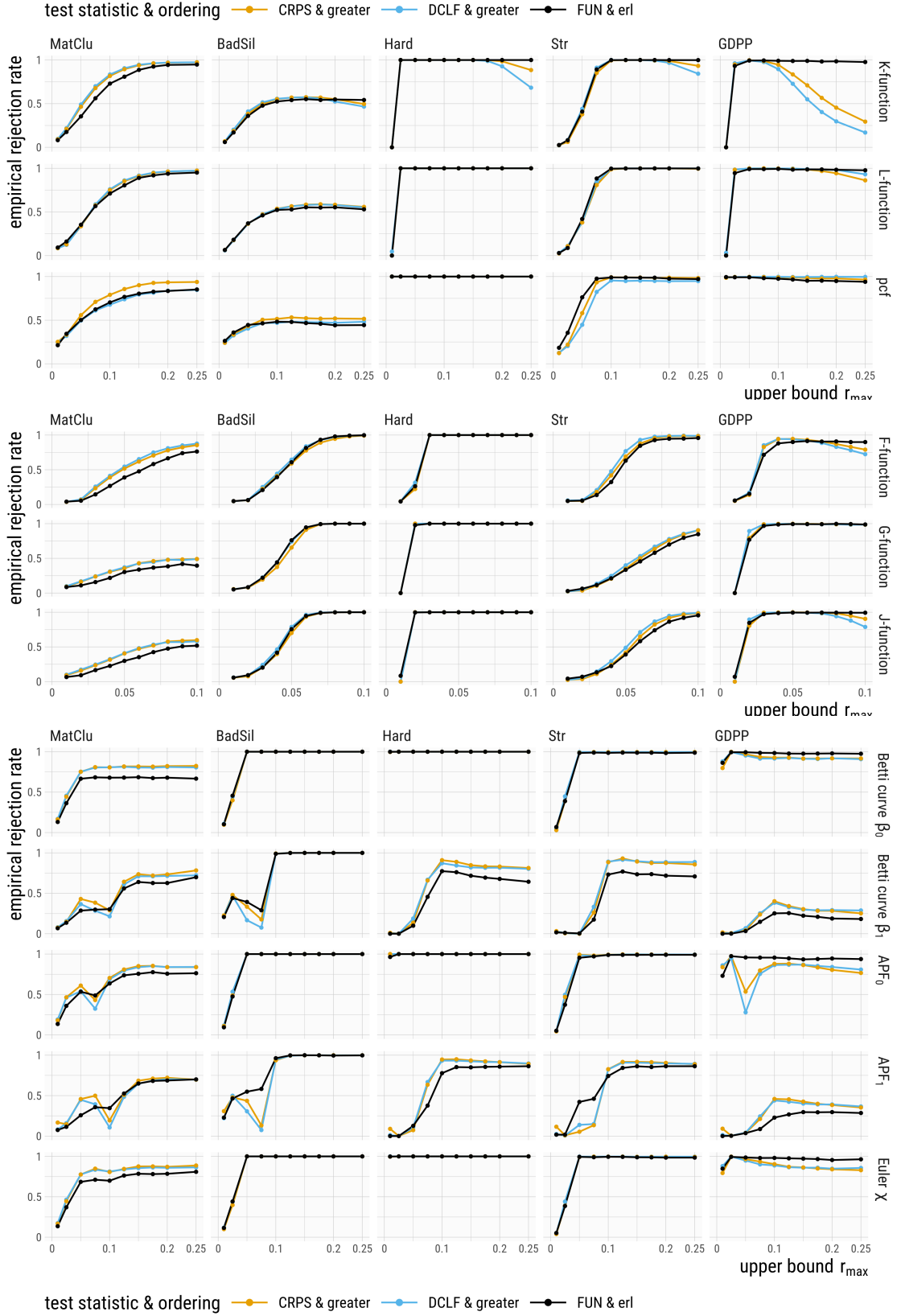


Figure 6: Empirical power curves for the test statistics CRPS, DCLF and FUN with the erl ordering with respect to the upper bound r_{\max} of the domain \mathcal{R}^* . We used $m = 299$ simulations on the observation window W_6 .

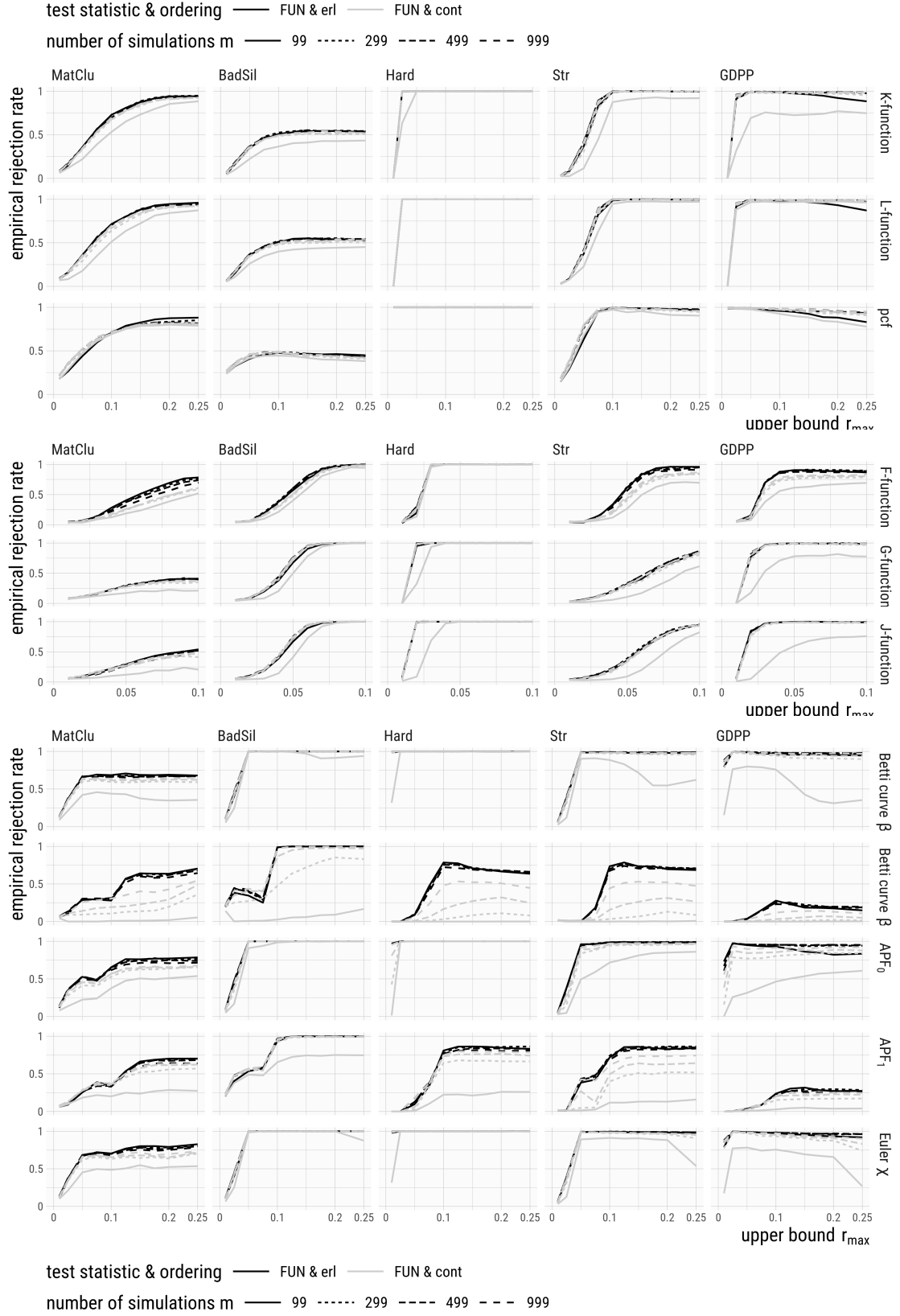


Figure 7: Empirical power curves for the test statistics FUN with either the erl or the cont ordering and varying number of simulations m on the observation window W_6 .

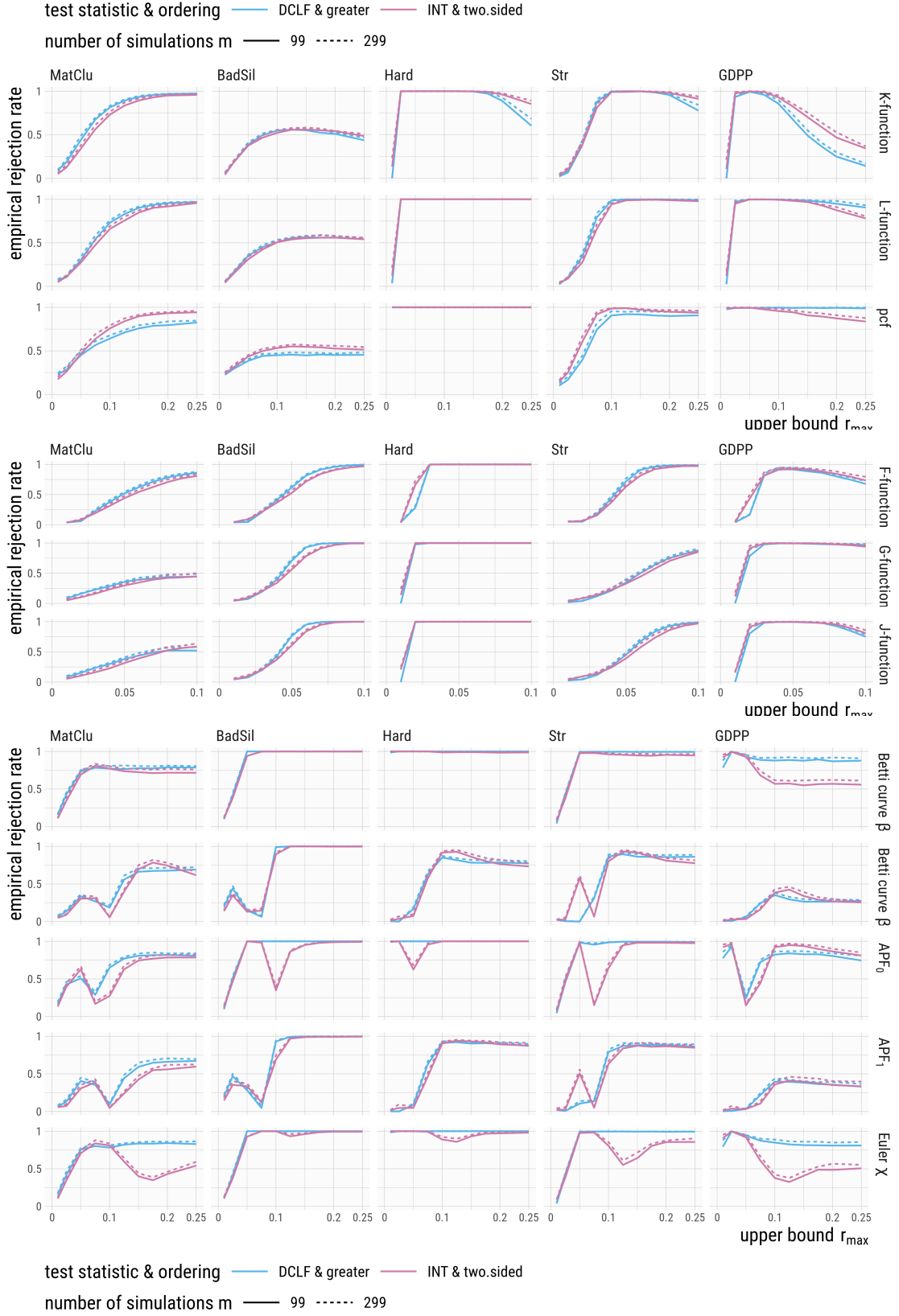


Figure 8: Empirical power curves with respect to the upper bound r_{\max} of the domain \mathcal{R}^* with observation window W_6 .

Appendices

A Continuous rank ordering for the 1-dimensional Betti curve

As mentioned in Section 5.1, the continuous rank ordering (cont) performs worse than the other orderings when the selected functional summary statistic is the 1-dimensional Betti curve β_1 . In this section, we discuss a small example which illustrates the problem.

The continuous rank measure was introduced in Mrkvička et al. (2022). The idea behind this ordering is to identify the extremeness of a curve via local extremeness over a small subset of the domain. Below, we provide the brief construction of the continuous rank.

Let $D_i = [D_i^{r_1}, \dots, D_i^{r_n}]$ denote the pointwise values of the discretized β_1 curve of the i th point pattern at n distinct evaluation points $r_1 < r_2 < \dots < r_n$. In total, we have $m+1$ vectors corresponding to $i = 0, \dots, m$ where $i = 0$ denotes the observed point pattern. We want to order these vectors using the continuous rank ordering.

For this ordering, first denote by $D_{(0)}^r \leq \dots \leq D_{(m)}^r$ the increasingly ordered $m+1$ values at evaluation point r .

If there are no ties involving the i th ordered value, then its raw continuous pointwise rank is defined to be

$$c_{(i)}^r = \begin{cases} \exp\left(-\frac{D_{(1)}^r - D_{(0)}^r}{D_{(m)}^r - D_{(1)}^r}\right) \cdot \mathbb{1}(D_{(1)}^r < D_{(m)}^r) & \text{if } i = 0, \\ i + \frac{D_{(i)}^r - D_{(i-1)}^r}{D_{(i+1)}^r - D_{(i-1)}^r} & \text{if } 0 < i < m, \\ m+1 - \exp\left(-\frac{D_{(m)}^r - D_{(m-1)}^r}{D_{(m-1)}^r - D_{(0)}^r}\right) \cdot \mathbb{1}(D_{(0)}^r < D_{(m-1)}^r) & \text{if } i = m. \end{cases} \quad (1)$$

If there are ties for the i th ordered value, i.e. there are some $k \neq l$ with $0 \leq k \leq i \leq l \leq m$ such that $k = \min\{0 \leq k' \leq i \mid D_{(k')}^r = D_{(i)}^r\}$ and $l = \max\{i \leq l' \leq m \mid D_{(l')}^r = D_{(i)}^r\}$, then the raw continuous rank is defined as

$$c_{(i)}^r = \frac{k + l + 1}{2}. \quad (2)$$

In our goodness-of-fit test, the pointwise continuous rank of curve i at evaluation point r is given as

$$C_i^r = \min(c_i^r, m+1 - c_i^r) \quad (3)$$

to take both large and small deviations into account.

In the next step, the pointwise continuous ranks are summarized in the continuous rank for the entire vector by taking the minimum of the pointwise ranks, i.e.,

$$C_i = \min_{r \in \{r_1, \dots, r_n\}} C_i^r \quad \text{for } i = 0, \dots, m. \quad (4)$$

Small values of C_i correspond to the most extreme curves, while the most central curves get the largest continuous ranks.

In our example, we consider one of the realizations of the MatClu model on the observation window W_6 . In our study, we were not able to reject the null hypothesis of CSR for this pattern when using the cont ordering, regardless of the number of simulations m . The corresponding pattern \mathbf{x}_0 is shown in Figure 9a. For demonstration purposes, we used only $m = 19$ simulations of the CSR null model in the Monte Carlo tests illustrated in the following. Since $m = 19$, we reject the null hypothesis for \mathbf{x}_0 if and only if $\beta_1(\mathbf{x}_0, \cdot)$ is the single most extreme curve.

The β_1 curves for the 20 point patterns used in the tests are shown in Figure 9b. The solid black line corresponds to the observed curve $\beta_1(\mathbf{x}_0, \cdot)$.

The graphical representations in terms of the global envelopes of the tests with test statistic FUN and the erl and the cont ordering are shown in Figure 9c and Figure 9d, respectively. In case of the extreme rank length ordering, we reject CSR, as the solid line leaves the gray envelope at at least one evaluation point ($p_{MC} = 0.05$). For the continuous ranks, we accept the null hypothesis ($p_{MC} = 0.3$). For this ordering, 5 point patterns (patterns $\mathbf{x}_6, \mathbf{x}_8, \mathbf{x}_{12}, \mathbf{x}_{15}$ and \mathbf{x}_{18}) of the 19 simulated patterns are deemed more extreme than \mathbf{x}_0 . Figure 10 shows for the six relevant point patterns all pointwise continuous ranks of the 1-dimensional Betti curves, as well as the evaluation point with minimal pointwise continuous rank.

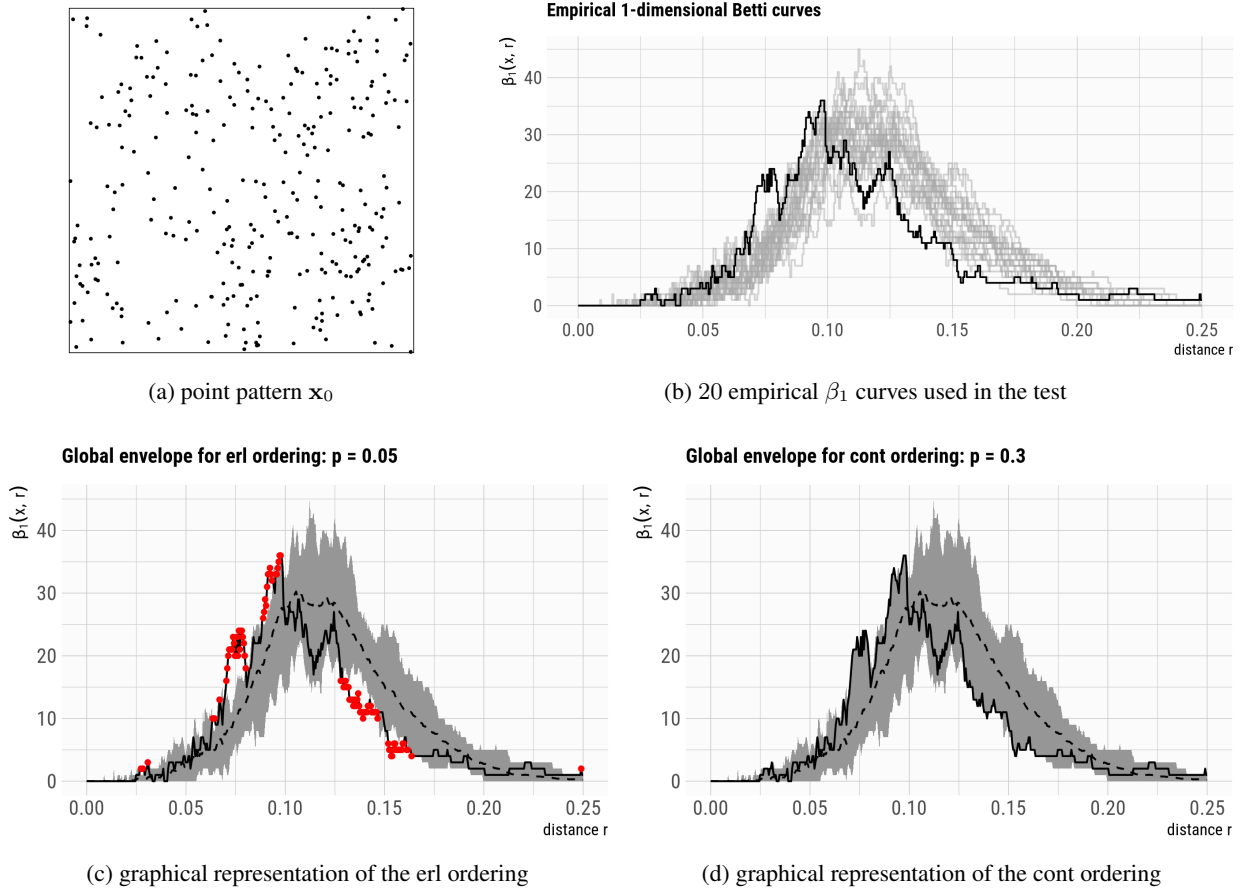


Figure 9: Visualization of the global envelope tests for the null hypothesis of CSR using the 1-dimensional Betti curve as functional summary statistic and either the erl or the cont ordering. The observed pattern shown in (a) is a realization of the MatClu model on the observation window W_6 . We used $m = 19$ simulations of CSR. All 20 curves are shown in (b) where the black solid line is the curve obtained from x_0 . The global envelopes corresponding to the test using FUN and the erl ordering (p -value = 0.05, rejection) and the one with the cont ordering (p -value = 0.3, acceptance) are shown in (c) and (d), respectively. The dashed line corresponds to the pointwise mean of the Betti curves. The red dots indicate which distances led to the rejection of the null hypothesis.

Let i be the index of one of the five simulated curves that are extreme under the cont ordering. There exists at least one evaluation point r for each curve where the pointwise continuous rank C_i^r for $\beta_1(x_i, r)$ is equal to 0. This results for each of the five curves in the overall value of the continuous rank of $C_i = \min_r C_i^r = 0$ which is the smallest possible continuous rank that can be achieved.

A continuous rank of 0 is also the reason that the observed curve coincides with the boundary of the global envelope for a large part of the domain.

For the global envelope as graphical representation of the test with significance level α , we first need to compute a threshold value ν_α . This threshold is the largest value of the individual continuous ranks such that the number of the continuous ranks strictly smaller than ν_α is at most $\alpha(m+1)$ (see Eq. (51) in Fend and Redenbach (2025) for details). In our example with $m = 19$, significance level $\alpha = 0.05$ and the existence of one continuous rank of 0 we obtain the threshold $\nu_\alpha = 0$. The global envelope shown in Figure 9d is finally formed by taking the pointwise minimal and maximal value of all curves where $C_i \geq \nu_\alpha = 0$. In our case, this results in taking the extreme values of all 20 1-dimensional Betti curves, the 19 simulated ones and the observed one.

We will now look in more detail at the cases in which $C_i^r = 0$ occurs. From (1), (2) and (3) it becomes clear that $C_i^r = 0$ can only be achieved if there are no ties involved, as otherwise the raw continuous rank c_i^r will never be 0 or $m+1$ due to the averaging. Additionally, due to the definition in (1) we see that the value of the corresponding Betti

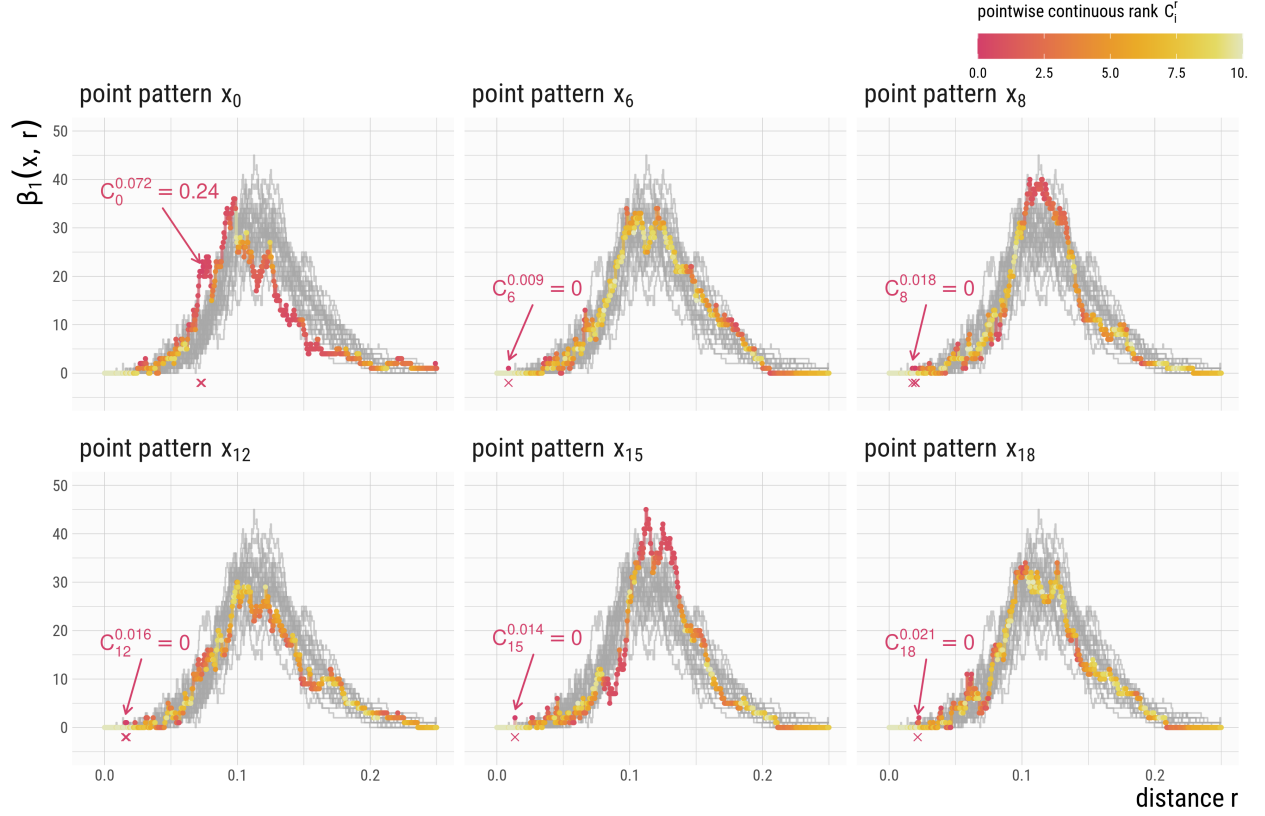


Figure 10: Pointwise continuous ranks C_i^r of the 1-dimensional Betti curves $\beta_1(\mathbf{x}_i, \cdot)$. Pattern \mathbf{x}_0 is the observed point pattern, patterns $\mathbf{x}_6, \mathbf{x}_8, \mathbf{x}_{12}, \mathbf{x}_{15}$ and \mathbf{x}_{18} have a smaller continuous rank than \mathbf{x}_0 and are hence more extreme. Small pointwise continuous ranks shown in red are hereby extreme while the yellow coloring with $C_i^r = 10$ corresponds to the most central pointwise values. The red crosses correspond to all evaluation points where $C_i^r \leq \min_r C_0^r = 0.24$ (the continuous rank measure of the observed point pattern).

curve at point r , i.e. D_i^r , needs to be either the largest or the smallest value, thus we are in the first or the last case. Since the exponential term is strictly positive, the indicator needs to be zero to get a raw continuous rank of either 0 or $m + 1$. We conclude in both cases that all the remaining m ordered values $D_{(1)}^r, \dots, D_{(m)}^r$ or $D_{(0)}^r, \dots, D_{(m-1)}^r$ need to coincide.

Thus, we only have two appearing values $d_1 \neq d_2$, with m curves attaining the one value d_1 and one curve (in our case the i th one) attaining the other value d_2 . This yields the pointwise and overall continuous rank for the i th curve of 0. Note that in this scenario, neither the absolute nor the relative difference between the two values is taken into account. In our example, we have $d_1 = 0$ and either $d_2 = 1$ (for the patterns $\mathbf{x}_6, \mathbf{x}_8, \mathbf{x}_{10}, \mathbf{x}_{18}$) or $d_2 = 2$ (pattern \mathbf{x}_{15}). Thus, the entire curves are considered more extreme because there exists some evaluation point where one or two 1-dimensional topological holes formed. These holes do not persist for a long time and would be considered topological noise in topological data analysis.

The corresponding alpha-complexes at the respective *extreme* evaluation points (as annotated in Figure 10) highlighting the small 1-dimensional topological features are shown in Figure 11.

This example illustrates why we need a higher number of simulations for the cont ordering – in contrast to the erl and area ordering – when the functional summary statistics has evaluation points where it is very likely that almost all curves attain the same value.

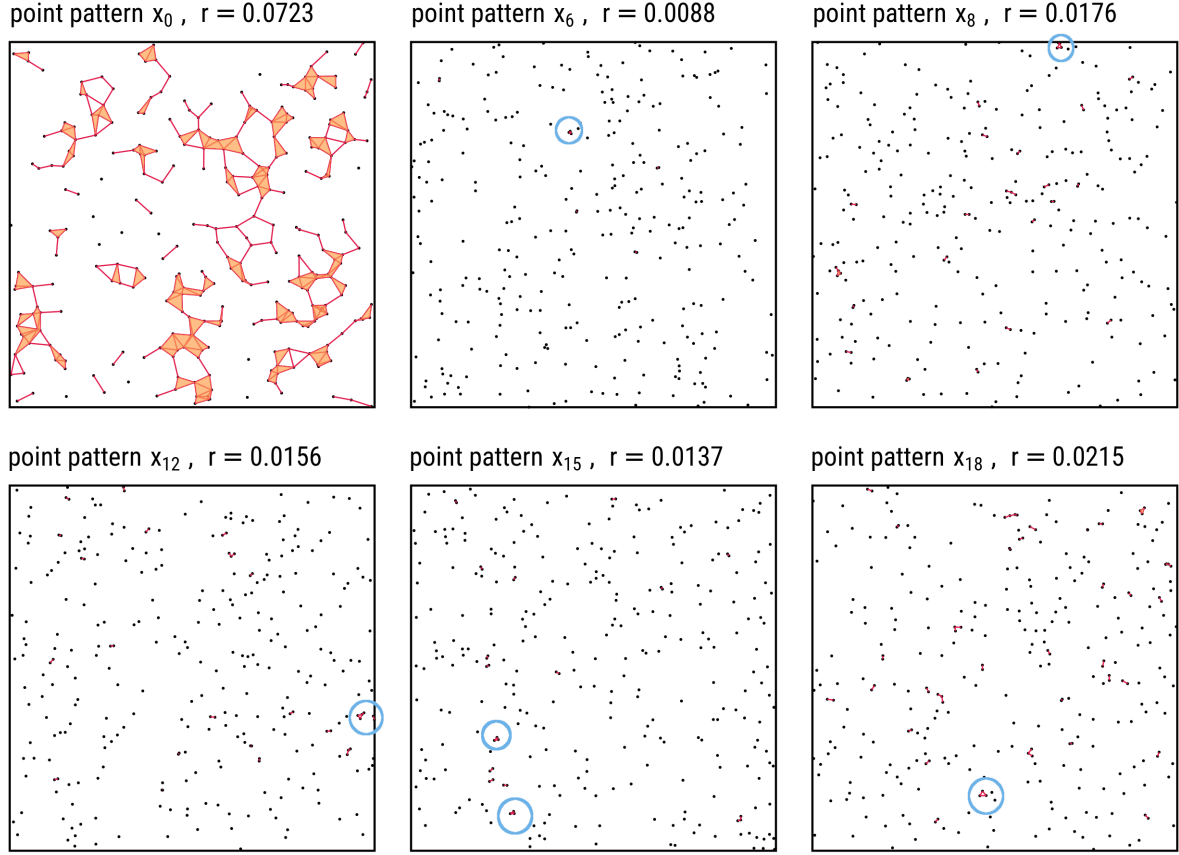


Figure 11: Alpha-complexes built on top of the point patterns at distance r . The distance for each pattern matches the distance where the minimal continuous rank of the 1-dimensional Betti curve is attained. The individual 1-dimensional topological features (circular holes) that exist in the complex are highlighted in blue in case they are hard to identify by eye.